Bangladesh's Accelerating Coastal Flood Hazard

Jiangchao Qiu[1*], Sai Ravela[1*] and Kerry Emanuel[1]

[1]Earth, Atmospheric and Planetary Sciences, Massachusetts Institute of Technology, 77 Massachusetts Avenue, Cambridge, 01239, MA, USA.

Abstract

The risk of extreme coastal flooding to Bangladesh's low-lying and densely populated coastal regions, already vulnerable to tropical cyclones, remains poorly quantified under a warming climate. Here, using a statistical-physical downscaling approach, our projections under the IPCC SSP5-8.5 scenario show that Bangladesh's 100-year coastal flood will likely intensify from **4.15**m to **6.60**m by the end of the **21**$^{\mathbf{st}}$ century. Meghna and northern Chattogram regions are the most vulnerable. The severity of coastal flooding season will broaden significantly, amplifying the strongest during the late monsoon season. Substantial increases are projected to seasonal coastal flood event frequencies, with a manifold increase in back-to-back flooding events in the post-monsoon season. We project that the frequency of coastal flooding from destructive cyclones like Bhola and Gorky will increase significantly. Our study heightens the urgency for attention and investment to enhance coastal resilience and mitigate risk in Bangladesh.

Keywords: Bangladesh, Coastal Floods, Storm Surge, Sea Level Rise, Climate Change

1 Introduction

Tropical cyclone (TC) induced coastal floods rank among the deadliest and costliest worldwide catastrophes [1]. The Bay of Bengal (BoB), located in the northeastern part of the Indian Ocean, has consistently experienced some of the most destructive coastal floods in history. Although it accounts for only 5-6 percent of global TC activity, approximately 80-90 percent of global TC fatalities occur in this basin [2, 3]. The BoB's funnel-shaped and shallow northern region naturally amplifies the water level, raising it to 10 meters above mean sea level when strong TCs strike [4, 5]. Six TCs in BoB have caused more than 140,000 fatalities [1] primarily due to coastal flood inundating the low-lying (less than 5 m above mean sea level) densely populated mega-delta [6] (with a population density of $6,734$ per km^2).

Bangladesh is a downstream riparian state for three major trans-Himalayan rivers, namely the Ganges, the Brahmaputra, and the Meghna, and is fringed by the BoB. Due to this location, the country is prone to coastal floods caused by intense TCs. It has a history of devastation caused by TCs, with 14 such events resulting in the loss of over 10,000 lives from 1760 to 2020 [7]. The latest of these was cyclone Gorky in April 1991, which claimed at least 13,000 lives. Sitting on the frontline in the battle against coastal floods, the country has since emerged as an international champion [8], implementing proactive policies to improve its resilience significantly. The government has improved its early warning system, increasing access to a network of cyclone shelters and evacuation roads, improving polders, and implementing community-based cyclone preparedness programs [9]. The results have yielded impressive results, reducing mortality from TCs by up to a hundred-fold. In May 2020, Super Cyclone Amphan hit the western coast of Bangladesh, resulting in a limited death toll of 128 despite inducing a 5 m storm surge [10].

However, a warming climate likely poses a significant threat to Bangladesh. The older embankment systems, which consist of 139 polders covering 1.2 million hectares of land, were built to protect about 8 million people from flooding and ensure their safety and livelihoods. However, if Sea Level Rise (SLR) and extreme TCs become more frequent and destructive due to climate change, the exposed infrastructure and vulnerable populations will be at greater risk. Increased sedimentation, elevating riverbeds, and land subsidence within polders increase embankment stress exposure to even low-intensity TCs. Furthermore, rising coastal water levels, reduced upstream river discharge, and polder-induced tidal amplification may worsen salinity intrusion. If the cyclone season expands into the monsoon season, the combined impact of coastal and inland flooding could devastate agriculture and water supply, further straining the vulnerable population.

The consequences faced by coastal Bangladesh are severe and often appear irreversible. The sustainability architecture of Bangladesh seems fragile in light of the emerging climate hazard. Risk-informed solutions are needed, and ones developed here could apply to many lower-income coastal countries worldwide. To make informed decisions, it is necessary to quantify the impact of climate change accurately. Focusing on TC-induced coastal flood risk, achieving this requires efficiently downscaling TCs to establish climatologies in future climate scenarios. This is challenging due to

the limited observational record of cyclones passing through Bangladesh and the enormous computational expense of running high-resolution numerical climate models. A previous study evaluated coastal flood risks using a synthetic simulation-based framework in Bangladesh [11]. However, this assessment is limited to the current climate. As of this writing, few TC-risk studies for Bangladesh under a changing climate exist.

Here, using a statistical-physical modeling framework to explicitly downscale TCs, we physically simulate coastal flooding for entire coastal Bangladesh under different projected climates [12–14]. Although other areas utilizing similar frameworks [15–18] have been studied, none has been established for BoB. Our approach investigates the effects of climate change (including TC climatology change and probabilistic SLR) utilizing a downscaled track set [7], which projects a ten-fold increase in the likelihood of extreme TC winds (exceeding 150 knots) by the end of the century under the high greenhouse gas emission scenario. The simulated synthetic TCs drive a validated hydrodynamic model [19] to simulate storm surges, including tides, using updated higher-accuracy regional bathymetry [20]. We estimate the return periods of coastal floods in current and future climates at stations along Bangladesh's coastline. We investigate the relative contribution of TC climatology change and SLR to coastal flooding across scales. We analyze the frequency that storms similar to the historically deadliest TC-induced coastal floods (Bhola and Gorky, tracks and fatalities can be found in Figure 1) might have in a warming climate. We further study seasonal shifts in flood severity and frequency.

Although some scenario uncertainty exists, under IPCC6 SSP5.85, our results are somewhat alarming. They provide important insight to help Bangladesh contend with climate change's mounting impacts on its coastal communities. To summarize our findings:

1. A national-scale assessment shows that the 100-year coastal flood in Bangladesh will likely intensify from the present 4.15 m (Confidence Interval [CI]: 2.63 m to 5.69 m. Hereafter, CI represents the confidence interval from 0.1 to 0.9 quantile) to 6.60 m (CI: 4.33 m to 9.68 m) by the end of the 21st century under CMIP6 SSP5-8.5.
2. Regional and station-level assessments show that Meghna and northern Chattogram are highly vulnerable. Under the warming climate scenario of CMIP6 SSP5-8.5, 100-year coastal flooding at the north part of Chattogram (simulated for virtual location named "station Navi" with ID=31 and marked by purple square in Figure **??**) will increase from the present 6.51 m (CI: 6.13 m, 6.89 m) to future 10.30 m (CI: 8.27 m, 12.45 m).
3. TC climatology, including frequency and intensity, amplifies more under CMIP6 SSP5-8.5 than under CMIP5 RCP8.5. Consequently, the increasing coastal flooding is dominated by TC climatology change under CMIP6 SSP5-8.5; specifically, TC climatology change contributes on average 71.6% (in the Ganges), 71.9% (in the Meghna), 63.2% (in the Chattogram) to the increasing coastal flooding for the 100-year return period.
4. Under CMIP6 SSP5-8.5, the return period of two historically deadliest coastal floods caused by TC Bhola (9.10 m) and Gorky (7.30 m) will decrease from present 623 years (CI: years 487 to 764) and 494 years (CI: years 396 to 597) to a future 47-year (CI: years 21 to 156) and 25-year (CI: years 16 to 108), respectively. In other

words, the frequency of storms like these extreme events increases by 13.3 (changing from 1 in 623 to 1 in 47) and 19.8 (varying from 1 in 494 to 1 in 25), respectively.

5. Climate change significantly broadens the TC active season, overlapping into the monsoon season robustly at multiple levels of severity. The cascading effect of inland and coastal flood risk in August poses a significant new danger. Seasonal coastal flood frequency significantly increases in October, leading to a higher likelihood of back-to-back coastal flooding due to the decreased time interval between occurrences.

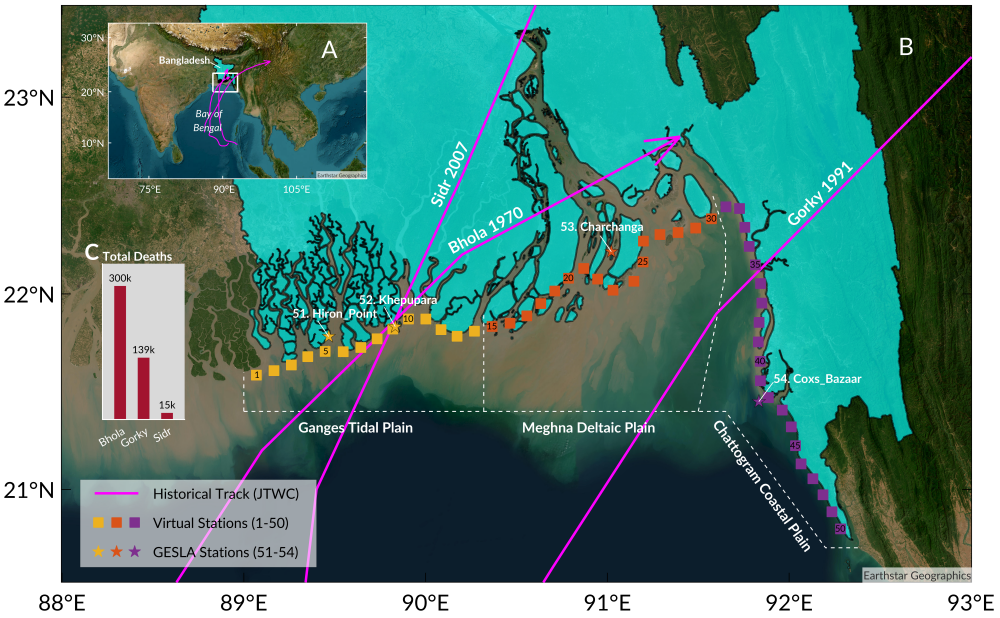

Fig. 1 Maps of historically deadliest TCs that made landfall in Bangladesh. A, Joint Typhoon Warning Center (JTWC) TC tracks (marked magenta with arrow) of Bhola (1970), Gorky (1991), and Sidr (2007) that originate in the Bay of Bengal and move northward, striking Bangladesh (marked cyan). **B**, zooming into coastal Bangladesh to display geographical locations where the three TCs made landfall and 54 water level "stations" located in Southwest Bangladesh (Ganges Tidal Plain, marked yellow), Middle Bangladesh (Meghna Deltaic Plain, marked orange) and East Bangladesh (Chattogram Coastal Plain, marked purple). Equidistant sampling is implemented along Bangladesh's coastline (300 km) to generate 50 points (defined as virtual stations) at 6 km intervals, supplemented by the only four existing GESLA tidal stations. Virtual stations are labeled with the MIT/Earth Signals and Systems Group alums' names, represented by squares with IDs from 1 to 50, while GESLA stations are represented by pentagrams with IDs from 51 to 54; detailed information for regional stations can be found in Table B2. **C**, the histogram with the associated number refers to the reported total fatalities caused by each TC (data from reference [21]). Base map sourced from the BDP 2100 (Baseline Volume 1, pg. 403), Humanitarian Data Exchange, World Bank, ESRI ArcGIS, Maxar, Earthstar Geographics, USDA FSA, USGS, Aerogrid, IGN, IGP, and the GIS User Community.

2 Results

2.1 Bangladesh's coastal floods under current and future climate across scales

We conducted coastal flood hazard assessments in Bangladesh to determine how climate change affects coastal flooding and which regions are most vulnerable. The assessments were carried out at national (aggregate projections for all 54 stations), regional (projections aggregated within stations in the Ganges, Meghna, and Chattogram, respectively), and local (station) scales. At the national level, we found that Bangladesh's coastal floods will significantly increase due to climate change by the end of the 21st century, see Figure A1. The 100-year coastal flood, currently at 4.15 m (CI: 2.63 m to 5.69 m), is projected to rise to 5.92 m (CI: 3.98 m to 8.97 m) and 6.60 m (CI: 4.33 m to 9.68 m) under CMIP5 RCP8.5 and CMIP6 SSP5-8.5 respectively. The less frequent 500-year coastal flood, currently at 5.47 m (CI: 3.45 m to 7.31 m), is expected to escalate to 7.28 m (CI: 4.97 m to 10.46 m) and 8.26 m (CI: 5.50 m to 11.35 m) under CMIP5 RCP8.5 and CMIP6 SSP5-8.5 respectively. Climate change exacerbates Bangladesh's 100-year and 500-year coastal floods, causing a rise of 1.77 m and 1.81 m under CMIP5 RCP8.5 and 2.45 m and 2.79 m under CMIP6 SSP5-8.5 respectively. The projections from CMIP6 models increase risk compared to CMIP5 models. Furthermore, the statistical uncertainty increases at more extended return periods.

Coastal floods in Bangladesh distribute unevenly under climate change. As shown in Figure 2 (regional scale), the 100-year flood in the Ganges is currently at 3.76 m (CI: 2.98 m to 4.84 m), but it is expected to increase to 5.47 m (CI: 4.10 m to 7.16 m) and 6.29 m (CI: 4.46 m to 8.51 m) under CMIP5 RCP8.5 and CMIP6 SSP5-8.5, respectively. The 100-year flood in the Meghna is expected to rise from 4.66 m (CI: 4.05 m to 5.97 m) to 6.91 m (CI: 5.49 m to 10.01 m) and 7.84 m (CI: 5.86 m to 10.17 m) under CMIP5 RCP8.5 and CMIP6 SSP5-8.5, respectively. In the case of Chattogram, the 100-year flood is expected to rise from 2.95 m (CI: 2.56 m to 6.18 m) to 4.81 m (CI: 3.70 m to 8.85 m) and 4.96 m (CI: 3.94 m to 9.85 m) under CMIP5 RCP8.5 and CMIP6 SSP5-8.5, respectively. Under CMIP5 RCP8.5, the 100-year flood values for the Ganges, Meghna, and Chattogram are expected to increase by 1.71 m, 2.25 m, and 1.86 m, respectively, while under CMIP6 SSP5-8.5, the increase values are 2.53 m, 3.18 m, and 2.01 m, respectively.

Figure A2 illustrates the projected 50-, 100-, and 500-year coastal floods at each station under CMIP5 RCP8.5 and CMIP6 SSP5-8.5. The CMIP6 increases are more significant compared to CMIP5 models. The coastal flood magnitudes are expected to increase the most at stations located in northern Chattogram. For example, at "station Navi" with ID=31, located at north Chattogram, the 100-year coastal flood is estimated to be 6.51 m (CI: 6.13 m to 6.89 m) under the current climate, 9.08 m (CI: 8.0 m to 11.13 m) under CMIP5 RCP8.5, and 10.30 m (CI: 8.27 m to 12.45 m) under CMIP6 SSP5-8.5. On the other hand, at "station Zhuchang" with ID=49, located at south Chattogram, the 100-year coastal flood is only projected to be 2.44 m (CI: 2.36 m to 2.52 m), 3.85 m (CI: 3.53 m to 4.90 m), and 4.41 m (CI: 3.73 m to 4.70 m) in the same scenarios. These findings suggest that northern Chattogram is the most vulnerable region to climate change, followed by Meghna in second place and

Ganges in third place. Southern Chattogram is ranked as the fourth most vulnerable region. The above assessment provides useful information for localized coastal climate adaptation planning and risk mitigation.

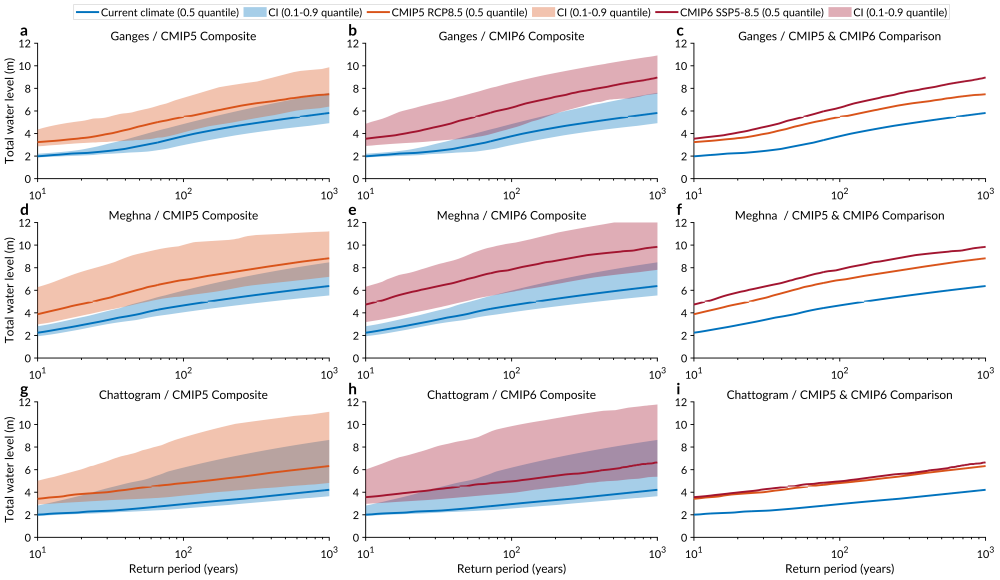

Fig. 2 Bangladesh's coastal floods versus return periods, as projected by CMIP5 and CMIP6 models at the regional scale. Coastal floods are the total water levels (combined components of astronomic tide, storm surge, and mean sea level state) relative to the mean sea level of the 1995-2014 baseline. **a, b, c,** Projections for the Ganges. **d, e, f,** Projections for the Meghna. **g, h, i,** Projections for the Chattogram. **a, d, g,** CMIP5 model ensemble composite, **b, e, h,** CMIP6 model ensemble composite. **c, f, i,** Comparison between CMIP5 and CMIP6 models. Blue, orange, and red solid lines indicate the ensemble median (0.5 quantiles) for the current climate, CMIP5 RCP8.5, and CMIP6 SSP5-8.5, respectively. Blue, orange, and red shaded areas indicate each estimate's confidence interval (CI, 0.1-0.9 quantile). The current climate period spans from 1981 to 2000, while the future climate period spans from 2081 to 2100.

2.2 The contributions of changing SLR and TC climatology to coastal flood risk

Changes in the coastal flood are influenced by two primary factors, TC climatology changes, and SLR, but their roles differ across Bangladesh's coastline. To measure the relative contribution of these factors to the increase in coastal flood, we compared the ensemble medians of coastal flooding (incorporating SLR, see Figure A2) and storm tide (without considering SLR, Figure B19) at each return period. The results, depicted in Figure 3, show that the proportion of coastal flood attributed to the change in TC climatology is greater under CMIP6 SSP5-8.5 than under CMIP5 RCP8.5. Interestingly, projections within CMIP6 SSP5-8.5 indicate that TC climatology has more impact (TC contribution greater than 50%) than SLR on coastal flooding.

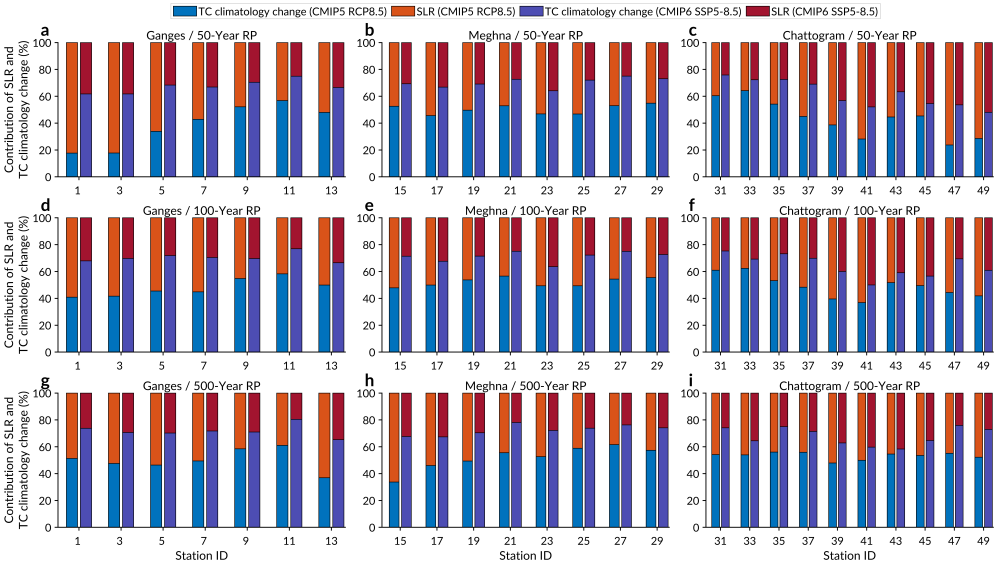

Fig. 3 Contribution of TC climatology change and SLR to changes of Bangladesh's coastal floods (50-year, 100-year, and 500-year return period) at the regional scale. a, b, c, 50-year return period. **d, e, f,** 100-year return period. **g, h, i,** 500-year return period. **a, d, g,** stations located in the Ganges. **b, e, h,** stations located in the Meghna. **c, f, i,** stations located in the Chattogram. Projections were conducted for all 54 stations; here, the graph only displays every other station. The blue and orange stacked histogram heights indicate the percentage of TC climatology change and SLR to changes of coastal flood projected by the CMIP5 models, respectively. The purple and red stacked histogram heights indicate the percentage of TC climatology change and SLR to changes of coastal flood projected by the CMIP6 models, respectively. The changes of the coastal flood are calculated based on these estimates' ensemble median (0.5 quantile).

Specifically, under CMIP5 RCP8.5, 42.6% (50-year return period), 48.2% (100-year return period), and 66.7% (500-year return period) of all 54 stations experience an increase in coastal flood predominantly caused by TC climatology change rather than SLR. On average, TC climatology change contributes 49.9% (in the Ganges), 52.6% (in the Meghna), and 47.0% (in the Chattogram) to the increase of coastal flood for the 100-year return period. In comparison, projections under CMIP6 SSP5-8.5 indicate that TC climatology changes dominate the growth of coastal flood in 94.4% (50-year return period), 100% (100-year return period), and 100% (500-year return period) of all 54 stations. On average, TC climatology change contributes 71.6% (in the Ganges), 71.9% (in the Meghna), and 63.2% (in the Chattogram) to the increase in coastal flood for the 100-year return period.

2.3 Frequency of historically deadliest coastal floods under warming climate

Estimating the annual exceedance frequency (the reciprocal of the return period) of the deadliest coastal floods in a future scenario similar to the deadliest TCs from the past, such as TC Bhola (1970) and TC Gorky (1991), is crucial for developing

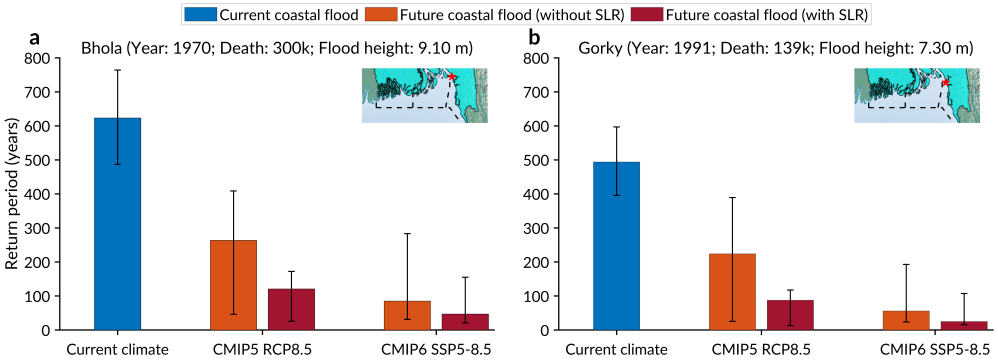

Fig. 4 Changing annual frequency of historically deadliest TC-induced coastal floods in a warming climate. a, assessment for the TC Bhola at "station Nick" with ID=32. **b**, assessment for the TC Gorky at "station Paco" with ID=34 (nearest to Chittagong). The histogram height indicates the ensemble median for the estimated return period of coastal flood corresponding to the observation (obtained from previous studies [1, 22, 23]). The whiskers indicate the estimated confidence interval (CI, 0.1-0.9 quantile). The red pentagram icon in the top-right corner of each subplot indicates the location where the maximum total water level was measured during the two landfall TCs. Base map sourced from the BDP 2100 (Baseline Volume 1, pg. 403), Humanitarian Data Exchange, World Bank, ESRI ArcGIS, Maxar, Earthstar Geographics, USDA FSA, USGS, Aerogrid, IGN, IGP, and the GIS User Community.

climate adaptation strategies. However, only one observation documents the maximum total water level during Bhola (9.10 m, observed at north Chittagong) [1, 22] and Gorky (7.30 m, followed near Chittagong) [23], respectively. Assessing risk across the entire coastline is challenging due to poor monitoring of water level records. Thus, we examine the 32nd station and 34th station (which are nearest to the observations) to represent approximately Bhola-induced and Gorky-induced maximum flood heights, respectively.

Figure 4 illustrates the annual frequency of these two deadliest TC-induced coastal floods in the current climate and their potential change in a warming climate, considering the joint effect of TC climatology change and SLR. In the current climate, the return period of Bhola's flood height is estimated to be 623 years (CI: years 487 to 764). By the end of the 21st century, projections under CMIP5 RCP8.5 show that it will become 264 years (CI: 46 to 408) without SLR and 121 years (CI: years 26 to 172) with SLR. Projections under CMIP6 SSP5-8.5 show that it will become 85 years (CI: 32 to 283) without the SLR effect and 47 years (CI: 21 to 156) with SLR.

Similarly, in the current climate, the return period of Gorky's flood height is estimated to be 494 years (CI: 396 to 597). By the end of the 21st century, projections under CMIP5 RCP8.5 show that it will become 224 years (CI: 26 to 390) without SLR and 88 years with SLR (CI: 14 to 118). Projections under CMIP6 SSP5-8.5 show that it will become 56 years (CI: 24 to 193) without and 25 years (CI: 16 to 108) with the SLR effect.

Thus, the annual frequency of the deadliest coastal floods, similar to those induced by Bhola and Gorky, is expected to increase significantly. The frequency of a Bhola-like flood height may increase from 1 in 623 to 1 in 47, while the frequency of a Gorky-like

flood height may increase from 1 in 494 to 1 in 25 under the CMIP6 SSP5-8.5 scenario. These projections consider the joint effects of TC climatology change and rising sea levels through joint Monte Carlo sampling (see Section 4.4 for explanation).

2.4 Changing seasonal intensity, frequency, and the summer monsoon season

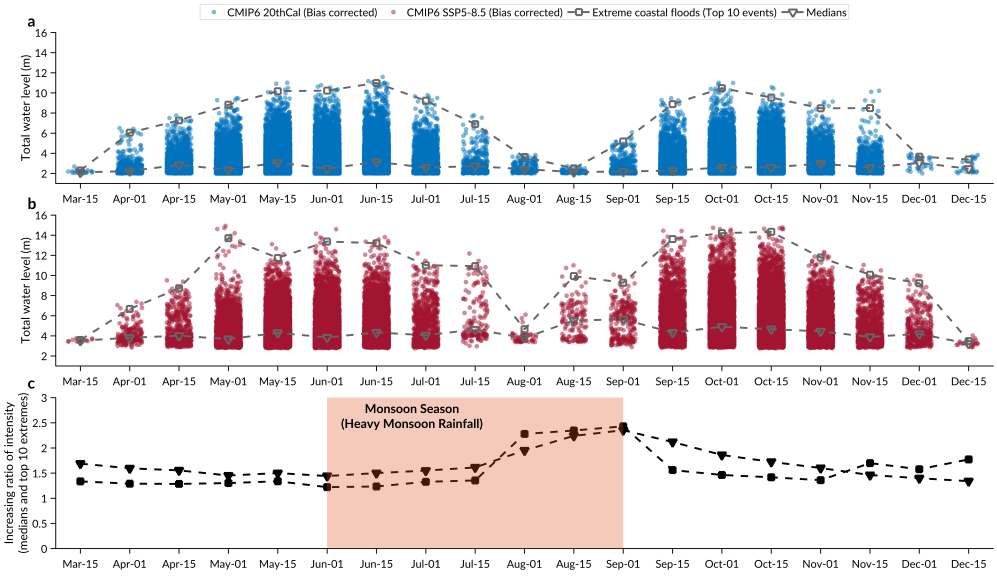

Fig. 5 Shifted seasonal regimes of coastal flood intensity (greater than 2 m flood height) based on CMIP6 climate model ensembles. a, seasonal distribution of coastal flood intensity under the CMIP6 current climate. **b**, seasonal distribution of coastal flood intensity under the CMIP6 SSP5-8.5 climate. **c**, the increasing ratio of median and extreme coastal flood intensities across the year, with a 3-point sliding average applied to get monthly ratios. The light gray square located at the top of each swarm in subplot **a** and **b** indicate the mean value of the top ten extreme coastal floods, while the light orange shading area in subplot **c** indicates the Monsoon season of the BoB.

Bangladesh's landfall TCs exhibit clear bimodal seasonality, typically active during the pre-monsoon period (April-May) and the post-monsoon period (October-December), but are relatively silent June–August) due to the strong vertical wind shear caused by the South Asian summer monsoon [24]. Here, we further investigate how climate change affects such seasonal coastal flood regimes in severity (Figure 5) and frequency (Figure 6).

Our findings suggest that the coastal flooding season will broaden significantly, with the strongest severity amplifying during the monsoon flooding season. Specifically, Figure 5 depicts a heightened coastal flood intensity and a broadened coastal flood season based on CMIP6 climate model ensembles. An inactive coastal flood season exists during the summer monsoon period, particularly from August 01 to September

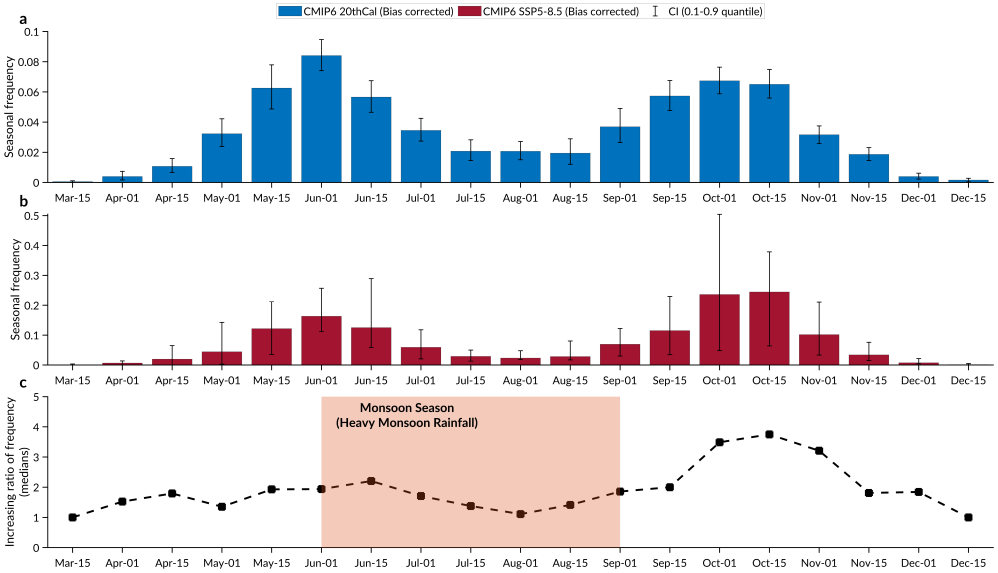

Fig. 6 Shifted seasonal regimes of coastal flood frequency (greater than 2 m flood height) based on CMIP6 climate model ensembles. a, seasonal of coastal flood frequency under the CMIP6 current climate. **b**, seasonal distribution of coastal flood frequency under the CMIP6 SSP5-8.5 climate. c, the increasing ratio of coastal flood frequency for the medians throughout the year. The error bar indicates the confidence interval from the 0.1 to 0.9 quantile. The light orange shading area in subplot **c** indicates the Monsoon season of the BoB.

01, under the current climate (subplot **a** of Figure 5). The intensity of coastal flooding during such three successive seasonal periods for the top ten extreme events are 3.63 m, 2.50 m, and 5.18 m. The corresponding ensemble medians are 2.42 m, 2.14 m, and 2.20 m, respectively. However, the coastal flood intensity during the same periods is projected to change significantly under the future climate to 4.66 m, 9.93 m, and 9.28 m for the extremes and 3.79 m, 5.53 m, and 5.64 m for the median flood. The intensity ratios increase significantly during these three seasonal periods compared to any other period, with values of 2.28, 2.35, and 2.43 for the ensemble extremes and 1.95, 2.24, and 2.35 for the ensemble medians, respectively. Climate change has significantly shortened the interval of cyclone dormancy from 45 days to a mere 15 days (only August 01). The heightened levels of coastal flooding during the late monsoon season (around mid-August) overlapping with the already existing heavy monsoon rainfall (e.g., the devastating floods of August 2017 [25]) can substantially amplify the cascading inland-coastal flood risk in Bangladesh.

In addition, there have been substantial changes to significant seasonal coastal flooding event frequencies, with a potentially manifold increase in back-to-back flooding events during post-monsoon seasons. Specifically, Figure 6 indicates the shifted seasonal frequency of coastal floods based on CMIP6 climate models. The combined impact of TC climatology change and SLR is causing an increase in the frequency of coastal floods that exceed a two-meter threshold. The most significant rise occurs

during the post-monsoon season, particularly in October. The seasonal frequencies of coastal flooding during the three successive periods are 0.067 (CI: 0.059 to 0.076), 0.065 (CI: 0.056 to 0.075), and 0.032 (CI: 0.026 to 0.038), respectively, under the current climate. However, these frequencies change to 0.236 (CI: 0.048 to 0.504), 0.244 (CI: 0.064 to 0.379), and 0.102 (CI: 0.033 to 0.211) under the future climate, with a significantly higher increase ratio of 3.49, 3.75, and 3.21 compared to any other seasonal period. More frequent events during each period will decrease the interval between occurrences, leading to a higher likelihood of back-to-back coastal flooding.

3 Discussion

Reliably estimating the frequency of extreme coastal floods is challenging, particularly in regions with insufficient observations, such as Bangladesh. Only limited studies have evaluated Bangladesh's coastal flood hazard under current climate conditions, let alone future ones. Khan [11] applied the same downscaling-hydrodynamic method to assess the coastal flood hazard in coastal Bangladesh, but only under the current climate. By comparing their result with other existing return period estimations, the author suggests that previous studies overestimate the coastal flood return period due to the biased extreme TC events sampling strategy. For example, Jakobsen [26] estimates that the 100-year flood height is about 5 m at the mouth of Meghna and about 8–10 m at Sanwip. In contrast, Khan's estimates are about 4 m at the mouth of Meghna and about 6 m at Sandwip. Our estimate in the current climate aligns with Khan's findings. We estimate that the 100-year flood height at the mouth of Meghna and Sandwip is about 4.66 m (Meghna region average) and 6.51 m ("station Navi" with ID=31), respectively. Regarding estimating the return period of coastal floods under future climate, only Leijnse [27] did some work in Bangladesh. The 100-year surge level estimated by Leijnse for Charchanga and Chittagong is over 60 cm lower than Khan's estimation. However, Leijnse's hydrodynamic model did not incorporate the updated bathymetric dataset in the northern BoB. Besides, only a purely statistical approach based on the historic TC dataset was applied to generate synthetic TCs without an explicit climate representation in addressing TC activity change under warming climates. As a result, significant uncertainties may remain in their coastal flood return period estimation. So, we do not make the comparison here.

Several noteworthy findings from our results deserve further discussion. First, our projections at the regional scale revealed that the increase in coastal flooding for Ganges (subplot **c** in Figure 2 and Figure B18) and Meghna (subplot **f** in Figure 2 and Figure B18) is higher under CMIP6 SSP5-8.5 than under CMIP5 RCP8.5. Still, there is no significant increase for Chattogram (subplot i in Figure 2 and Figure B18) from CMIP5 RCP8.5 to CMIP6 SSP5-8.5. Using a box plot, we display the distribution of 100-year storm tides for three regions under current and future climates (Figure B20). Compared to Ganges and Meghna, Chattogram shows a significantly right-skewed (the median closer to the box's bottom) and dispersed (extended box) distribution. The orientation of Chattogram, which runs parallel to the longitude, results in considerably different magnitudes of storm surges and tides (subplot **c**, **f**, **i** in Figure A2 and Figure B19) between the northern funnel top (station ID from 31 to 37) and the

remaining southern area (station ID from 38 to 50). The effect of TC climatology change on coastal floods in the south of Chattogram is relatively limited compared to other regions, regardless of whether it is under CMIP5 RCP8.5 or CMIP6 SSP5-8.5. *Sai comment: talk to me about coastally trapped waves in the BoB morphology. Remove this red flag before submission!*

Interestingly, TC climatology change contributes more than SLR to the elevated coastal floods under CMIP6 SSP5-8.5 compared to under CMIP5 RCP8.5. This difference results from the magnitude of TC climatology change because the same SLR samples were applied to CMIP5 RCP8.5 and CMIP6 SSP5-8.5. TC frequency is notably higher under CMIP6 SSP5-8.5, as illustrated in Figure A4, with a median of 1.58 (CI: 0.62 to 2.29), compared to CMIP5 RCP8.5, with a median of 0.88 (CI: 0.53 to 1.44). Equation 1 and Equation 2 show an inverse relationship between TC frequency and exceedance probability. As depicted in Figure A8, the total water level and exceedance probability also share an inverse relationship. An increase in TC frequency with a fixed return period T leads to a decrease in exceedance probability, ultimately resulting in a higher total water level. On the other hand, Emanuel's [7] TC wind projections in Bangladesh show that TC wind intensity increases significantly more under CMIP6 SSP5-8.5 than under CMIP5 RCP8.5. The 100-year TC wind rose from 123 knots to 145 under CMIP5 RCP8.5 while further escalating to 168 knots under CMIP6 SSP5-8.5. Therefore, CMIP6 SSP5-8.5 projects more frequent and intensified TCs than CMIP5 RCP8.5. As a result, we posit that TC climatology change under CMIP6 SSP5-8.5 contributes more to the growth in coastal flooding than under CMIP5 RCP8.5.

Our study has broad implications. We estimate the return period of coastal floods incorporating the combined effect of future TC climatology change and SLR and investigate flood distributions across seasons in intensity (severity) and frequency. Our assessment could inform the relevant policymakers and stakeholders about when and where to enhance coastal resilience further and mitigate risk towards more targeted and practical solutions in a changing climate. Our findings suggest that future planning, rehabilitation, and improvement of infrastructure investments should prioritize the region of Meghna and northern Chattogram and pay more attention to the growing risk of cascading inland-coastal flooding during late summer monsoons (August) and back-to-back coastal floods during the post-monsoon-period-(-October-and early November). Examples of such investments include the Coastal Embankment Improvement Project (CEIP) and Multipurpose Disaster Shelter Project (MDSP) from World Bank [9]. Accurately estimating extreme coastal floods' occurrence probabilities and seasonal distribution and implementing a well-designed risk mitigation plan can save livelihoods and reduce financial burdens by minimizing disaster impact while avoiding unnecessary and costly overprotection measures [28].

There are a few limitations in this study that require further improvement. Firstly, significant uncertainty exists among the various climate models that predict future TC activity [29] and SLR [30]. Although the newer CMIP6 has reduced these uncertainties compared to CMIP5, there is still a need for future research to improve the accuracy of these models in projecting the atmospheric and oceanic variables that control TC activity and sea level dynamics. Secondly, it's important to note that TCs

induce storm surges and produce extreme precipitation, especially when they stall during landfall. Emanuel [7] projects a twenty-fold increase in severe storm accumulated rainfall (exceeding 1000 mm in Dhaka) due to climate change. The growing overlap with the monsoon season is indicated here, and summer heat stress is shown elsewhere [] *Sai Comment: cite the nature paper on heat stress and cyclones.* Future research should consider these factors jointly in Bangladesh for integrating coastal, fluvial, and pluvial processes components [31–33], in addition to the compound effects of TC winds and rainfall that is well underway in the community.

4 Methods

Our approach involves three primary components: synthetic TC downscaling, hydrodynamic simulation, and statistical analysis incorporating bias correction. These components are discussed in this section.

4.1 Synthetic TC downscaling

We use a statistical-deterministic downscaling technique to create sets of synthetic tropical cyclones (TCs) that affect Bangladesh [12, 13]. The method uses thermodynamic and kinematic statistics from gridded global reanalyses or climate models to produce many synthetic TCs. Initially, we synthetically generate large-scale environmental factors such as potential intensity, wind shear, humidity, and thermal ocean stratification from gridded global reanalyses or climate models. These factors are created as a Fourier series of random phases in time, and they are constrained to have accurate monthly means, variances, and covariance with a geostrophic turbulence power-law distribution of the kinetic energy spectrum.

The time-evolving environment is seeded randomly in space and time with warm-core vortices of 12 m/s (25 knots) peak wind speeds. These seed vortices are then propagated forward with a weighted average of synthesized winds at the 250 and 850 hPa levels, according to the beta-and-advection model [34]. The intensity of the vortices is then calculated deterministically using the Coupled Hurricane Intensity Prediction System (CHIPS) model [35], which phrases the dynamics in angular momentum coordinates that allow for very high spatial resolution in the storm core. The intensity model also accounts for salinity effects on density, affecting TC potential intensity, since the Bay of Bengal has strong salinity gradients, especially in summer [7].

Over 99% of the seeded tracks dissipate quickly and are discarded. The remaining successfully grow to make up the downscaled TC climatology of a reanalysis or climate model. Only the seeds that develop a maximum wind speed of at least 21 m/s (40 kt) during their lifetime form synthetic TCs. The annual frequency of TC is postulated to be directly related to the ratio of successful to unsuccessful seeds in a given year, with a constant of proportionality established by comparing time averages to dependable historical records.

We identify synthetic TCs affecting Bangladesh based on their passage over one or both of the two-line segments displayed in Figure A3. ECMWF/ERA5 and GMAO/MERRA2 climate reanalyses yield 4,100 TCs for the current period (1980-2020). We also generate 2,000 TCs using six CMIP5 and seven CMIP6 global climate

models for two time periods: 1981-2000 for historical simulations and 2081-2100 for RCP 8.5 (CMIP5) and SSP5-8.5 (CMIP6) simulations. Overall, we generated a total of 60,800 TCs. Further details about this study's reanalyses and climate models are summarized in Table A1.

The annual frequency of historical TC landfall in Bangladesh is estimated to be 0.634 based on the 26 events recorded in the JTWC dataset from 1980 to 2020 [36]. We considered only those TCs with peak wind speeds more than the tropical storm intensity threshold (33 knots). We assume that this occurrence rate (0.634) represents the TC annual frequency under the current climate and that TC occurrence follows a Poisson process with arrival rate λ. More details about the landfall information and Poisson distribution fitting can be found in Figure A3.

Climate model projections may be biased; hence, we bias-correct the TC annual frequency for each climate model under the current climate through a multiplicative factor to match the observed annual frequency (0.634). Assuming that the bias correction calculated under the current climate can be applied to future projections, we multiply the frequency prediction for future climate by the ratio of the bias correction for the current climate. The original TC annual frequency for the future produced from the TC model is shown in Figure A4. The bias-corrected frequency and change information are presented in Section 4.4. However, the significant variation among the model predictions reflects the general uncertainties in climate model projections of TC frequency due to systematic model differences and internal climate variability [37].

4.2 Hydrodynamic simulation

Mesh generation.

We used ADCIRC (ADvanced CIRCulation model, two-dimensional barotropic tides, Version 55.01) [19, 38, 39] for storm surge simulations and used a tool called OceanMesh2D, to generate detailed, high-fidelity unstructured meshes [40, 41] for BoB (spanning latitudes from 9°N to 23°N and longitudes from 80°E to 100°E). The mesh generated by OceanMesh2D is based on several feature-driven geometric and topographic-bathymetric mesh size functions, providing adequate resolution to capture the intricate coastal characteristics.

To generate the computational mesh, *sai comment: fix this sentence* we used shoreline and bathymetry data. The shoreline boundaries were defined using the full-resolution Global Self-consistent Hierarchical High-resolution Shorelines (GSHHS) dataset [42]. Bathymetry data were obtained from two sources: the General Bathymetric Chart of the Oceans (GEBCO) on a 15 arc-seconds geographic latitude and longitude grid for the primary Bay of Bengal [43] and an updated bathymetric dataset for the Bengal Delta [20]. The bathymetric points were first mapped onto a structured grid at 200 m resolution using a simple kriging method [44]. Both bathymetries were unified to mean sea level. Bathymetry and bathymetric slope were interpolated onto inner and outer mesh vertices directly from the original DEM, then merged to ensure consistency across the connected areas (Figure B10).

The final unstructured mesh consisted of 62,009 vertices and 115,199 triangular elements, with a resolution ranging from 20 km over the deep ocean to 1 km near the coastlines (Figure A5). The mesh size functions and their corresponding parameter

values for spatially distributing element resolution are summarized in Table B3. The maximum topographic gradient was kept below 0.1 to ensure numerical stability. We used the information from shoreline distance and water depth to categorize the outer node string boundary into mainland and ocean. The ocean boundaries are the segments whose distance from the shoreline is beyond 0.4 geographic degrees, and the depth from the sea level is below 30 m (Figure B11). For the mainland boundary, the segments whose distance from the shoreline is within 0.4 geographic degrees and the depth from the sea level is below 30 m are classified as the mainland boundary.

Model setup.

Both astronomical tides and meteorological factors cause coastal floods. To obtain more precise and comprehensive astronomical tide solutions, all eight major astronomical tidal components (K_1, K_2, M_2, N_2, O_1, P_1, Q_1, and S_2) are taken into account. The self-attraction, loading, and internal tide terms are also considered [45, 46]. Astronomical tidal amplitudes and phases are obtained from the latest global satellite-assimilated tidal model TPXO9-Atlas-v5 with a resolution of 1/30° [47]. The surface wind and atmospheric pressure field associated with a TC is reconstructed at each node using the symmetric Holland parametric vortex model (H80) during the simulation [48]. The bottom friction is parameterized using *Manning's N*, with a similar approach to previous studies for the spatial distribution of the Manning coefficient to ensure consistency with them [10, 11, 20]. For water depths greater than 20 m, the Manning coefficient is 0.02, while it is 0.013 in the nearshore zone (Figure B12). To balance computational cost and numerical stability, a time step of 60 seconds is used for the simulation. Each simulation for one track takes approximately 8.8 seconds using a parallel setup with 40 CPU cores (Figure B13). For simulating multiple synthetic TCs, the timing of astronomical tides is synchronized with that of the synthetic TC, and a one-day model spin-up is applied for all simulations.

Model validation.

The hydrodynamic model's performance was assessed by comparing its output with TPXO9-Atlas and tide gauge station data for global astronomical tide validation and total water level validation, respectively, along the coast of Bangladesh. The model was initially driven by five leading astronomical tidal constituents (M_2, S_2, N_2, K_1, and O_1) for 31 days, with three days for spin-up and 28 days for harmonic analysis [44]. The model results showed the global responses of M_2 and K_1 tidal waves (Figure B14) and their RMSE discrepancies against TPXO9-Atlas (Figure B15) [39]. In comparison with previous studies [49, 50], the model accurately described the constituents' general response, including the amphidromes' positions.

Subsequently, the historical TC Sidr ("IO062007") was used to validate the total water levels. The results showed that the observed and simulated storm tides had satisfactory agreement, with an overall root-mean-square error, bias, and Willmott skill of 0.27, -0.09, and 0.96, respectively, at the Hiron Point (PSMSL ID=1451) and 0.43, -0.32, and 0.93, respectively, at the Khepupara station (PSMSL ID=1454) (Figure A6). The maximum water elevation during Sidr's lifetime can be found in Figure B16. Through this comprehensive validation process, we aimed to assess the hydrodynamic model's performance and ensure that it is suitable for capturing storm surge dynamics and water level variations in coastal Bangladesh.

4.3 IPCC AR6 relative sea-level projection

The probabilistic, localized relative sea-level projections are based on a Framework for Assessing Changes To Sea-level (FACTS) [51], which emphasizes the role of the Antarctic and Greenland ice sheet as drivers of structural uncertainty in sea-level rise projections. FACTS can generate seven alternative probability distributions relative to a 1995-2014 baseline under multiple alternative emissions scenarios presented in the Intergovernmental Panel on Climate Change Sixth Assessment Report (IPCC AR6) [30]. In this study, we apply the gauge-based Monte Carlo samples (20,000 in total) of future relative sea level under workflows 2-E and scenario SSP5-8.5, covering the period from 2080 to 2100 (Figure A7). The four gauge-based stations located in coastal Bangladesh are Hiron Point (PSMSL ID=1451), Khepupara (PSMSL ID=1454), Charchanga (PSMSL ID=1496), and Cox Bazaar (PSMSL ID=1476). The workflow 2-E of FACTS employs Gaussian Process emulation for Greenland, glaciers, and Antarctica and forms the basis of the *medium confidence* projections presented by IPCC AR6. The SSP5-8.5 emission scenario aligns with the scenario of TC projections in future climate and represents a high-end trajectory that would require a reversion to fossil-fuel-intensive development.

Previous studies used a convolution method to calculate the cumulative distribution function of a coastal flood, incorporating sea level rise (SLR). Still, we apply a sampling strategy considering the joint distribution with SLR. To do this, we pair each TC-induced peak storm tide with an SLR sample randomly selected from the Monte Carlo samples of sea-level projections. As we generate synthetic TCs year by year (100 per year) with explicit timing, we obtain an SLR sample for the same year for the gauge station closest to the TC landfall location among the four available GESLA gauge stations, adding it to the peak storm tide to represent the total water levels of the coastal flood. We also assume that the sea level rises monotonically. Thus, we represent the distributions using statistics at 2080, 2090, and 2100, linearly interpolated to the year to get SLR samples.

4.4 Statistical analysis

Return period estimation.

We calculate storm tide against return period curves (without considering sea level rise) and coastal flood against return period curves (including sea level rise) for each of the 54 coastal stations. For each simulation of coastal flood induced by a TC, we extract the highest water elevation during the entire cyclone's lifetime and the corresponding time. At each station, we use a vector of 2,000 peaks (climate model) or 4,100 peaks (climate reanalyses) for return period curve calculations. On the other hand, we use peak times to analyze the temporal distribution of extreme coastal floods. We assume that TCs arrive as a stationary Poisson process in a given climate [14]. We calculate the return period of TC-induced storm tides, which incorporates storm surge and astronomical tide but not SLR, exceeding a given return level h using the formula [52]:

$$T_{\eta_{\text{storm\_tide}}}(h) = \frac{1}{\lambda \times EP\{\eta_{\text{storm\_tide}} > h\}} \tag{1}$$

Where λ is the TC annual frequency, $EP\{\eta_{\text{storm\_tide}} > h\}$ is the annual exceedance probability of maximum TC-induced storm tide, $EP\{\eta_{\text{storm\_tide}} > h\} = 1 - P\{\eta_{\text{storm\_tide}} \leq h\}$, $P\{\eta_{\text{storm\_tide}} \leq h\}$ is the cumulative distribution function. Extreme value theory suggests estimating the probability of TC-induced storm tide using the Peaks-Over-Threshold method, with a Generalized Pareto Distribution in the upper tail [53]. This study divided the peak storm tide values into two segments using a fixed threshold at the 98th percentile. Then, we utilized the Generalized Pareto Distribution to fit the upper tail and a kernel density estimate [54] to fit the remaining portion (Figure A8). The cumulative distribution function at 100 equally spaced points is first estimated for smooth kernel density estimate. Then linear interpolation is used to compute the cumulative distribution function estimates for the points between the 100 points (function *paretotails* in MATLAB). Given a return period ranging from 10 to 1000, the corresponding return levels for storm tide can be calculated using the inverse cumulative distribution function (function *icdf* in MATLAB).

Once the contributions of SLR are included, the return period of the coastal floods (incorporating storm surge, astronomic tide, and SLR) exceeding a given return level h are calculated using the same method as storm tides by [52]:

$$T_{\eta_{\text{coastal\_flood}}}(h) = \frac{1}{\lambda \times EP\{\eta_{\text{coastal\_flood}} > h\}} \tag{2}$$

Where the annual exceedance probability of maximum coastal flood denoted as $EP\{\eta_{\text{coastal\_flood}} > h\}$, is defined as $EP\{\eta_{\text{coastal\_flood}} > h\} = 1 - P\{\eta_{\text{coastal\_flood}} \leq h\}$, where $P\{\eta_{\text{coastal\_flood}} \leq h\}$ is the cumulative distribution function.

The approach allows straightforward impact assessments of TC climatology change and SLR on future coastal floods at the station scale. The contribution of TC climatology change on coastal flood can be measured by the ratio of the water level (ensemble median) changes with and without considering the effect of SLR on the water level. After obtaining return period curves, we can determine the annual frequencies (the inverse of the return period) of the historical extreme total water levels based on return period curves under the current climate using observed flood heights. Furthermore, based on return period curves under future climate (with and without SLR), we can also predict the evolution of historical extreme flood frequency in a warming climate.

Bias correction.

It's important to note that climate model projections can be biased in various ways. These include estimating TC frequency, calculating return period curves for storm tide/coastal flood, and the seasonal distribution of TCs.

The annual frequency of TCs adjusts with a bias correction and differs depending on the climate model used (- means decrease while + means increase). CMIP5 models: GFDL5 is 0.53 (-6.59%), MPI5 is 0.56 (-2.67%), CCSM4 is 0.80 (+41.03%), IPSL5 0.95 (+67.19%), HADGEM5 is 1.16 (+103.51%), MIROC5 is 1.47 (+157.14%); for 7 CMIP6 models: CANESM is 0.59 (-7.44%), MPI6 is 0.74 (+16.93%), MRI6 is 1.18 (+86.44%), MIROC6 is 1.58 (+148.67%), CNRM6 is 2.15 (+239.61%), IPSL6 is 2.27 (+257.30%), ECEARTH6 is 2.30 (+262.89%).

We use a quantile-quantile mapping method to bias correct the data to ensure that our storm tide/coastal flood return period curves are accurate (Figure **??**). This is done station by station by adjusting the climate model-based return level to the

averaged reanalyses-based (ECMWF/ERA5 and GMAO/MERRA2) return level for the current climate in yearly return period increments. This produces a bias correction table for each station, return period, and climate model. The bias is also removed from each corresponding climate model in a future climate scenario, assuming that such bias must be removed to the first order.

We also bias-correct the seasonal distribution of coastal floods under current and future climates. This helps us investigate the seasonal shift regimes of coastal floods in intensity and frequency. The downscaling synthetic TCs with physics-consistent times allows for determining the specific date associated with the peak storm tide. We establish a 14-day window, including seven days before and seven days after each month's onset and middle days, to categorize the bias-corrected coastal floods into different seasonal periods. The frequency of flooding in a specific season is calculated by multiplying the annual frequency by the seasonal factor, representing the proportion of this season's coastal floods out of all coastal floods. Then, we align the current climate model frequency over 24 15-day periods with corresponding averaged reanalyses-based (ECMWF/ERA5 and GMAO/MERRA2) frequencies and apply the estimated bias correction for each relevant model and period in future seasonal frequency assessment.

5 Data availability

Some public data sets used for this study are available at https://www.soest.hawaii.edu/pwessel/gshhg/ (GSHHS), https://www.gebco.net/ (GEBCO), https://www.metoc.navy.mil/jtwc/jtwc.html?north-indian-ocean(JTWC), ftp://ftp.legos. obs-mip.fr/pub/FES2012-project/data/LSA/FES2014/ (FES tidal database), https://www.tpxo.net/global/tpxo9-atlas (TPXO9-atlas-v5), https://github.com/rutgers-ESSP/ipCC-AR6-Sea-Level-Projections (IPCC AR6 Sea-Level Projections), https://surge.climate.lsu.edu/data.html (SURGEDAT). WindRiskTech L.L.C. performs TC-induced risk assessments for clients worldwide and provides datasets for scientific research upon request (info@windrisktech.com), subject to a non-redistribution agreement. Our coastal flood frequency estimation will be publicly available upon acceptance of our manuscript.

6 Code availability

The hydrodynamic model is developed using the OceanMesh2D toolbox (https://github.com/CHLNDDEV/OceanMesh2D). The Peaks-Over-Threshold based Generalized Pareto Distribution fitting is executed using a MATLAB (Version 2022a) *paretotails* function. All figures are also generated using MATLAB. The codes used to create an unstructured mesh, make ADCIRC input for files, and result visualization can be accessed from the corresponding authors upon reasonable request.

7 Acknowledgment

Funding is gratefully acknowledged from the MIT Climate Resilience Early Warning Systems Climate Grand Challenges project, the Jameel Observatory JO-CREWSNEt

project, and the generosity of Eric and Wendy Schmidt by recommendation of Schmidt Futures as part of its Virtual Earth System Research Institute (VESRI). The authors thank Crystal Fulcher for providing the latest source code of adcirc_v55.01 and Y. Krien for offering the improved bathymetric dataset for the Northern Bay of Bengal.

References

[1] Needham, H.F., Keim, B.D., Sathiaraj, D.: A review of tropical cyclone-generated storm surges: Global data sources, observations, and impacts. Reviews of Geophysics **53**(2), 545–591 (2015)

[2] Chowdhury, K.: Cyclone preparedness and management in bangladesh. Improvement of early warning system and responses in Bangladesh towards total disaster risk management approach **115**, 119 (2002)

[3] Paul, B.K.: Why relatively fewer people died? the case of bangladesh's cyclone sidr. Natural Hazards **50**, 289–304 (2009)

[4] Islam, T., Peterson, R.E.: Climatology of landfalling tropical cyclones in bangladesh 1877–2003. Natural Hazards **48**, 115–135 (2009)

[5] Dasgupta, S., Huq, M., Khan, Z.H., Ahmed, M.M.Z., Mukherjee, N., Khan, M., Pandey, K.D.: Vulnerability of bangladesh to cyclones in a changing climate: Potential damages and adaptation cost. World Bank Policy Research Working Paper (5280) (2010)

[6] Streatfield, P.K., Karar, Z.A.: Population challenges for bangladesh in the coming decades. Journal of health, population, and nutrition **26**(3), 261 (2008)

[7] Emanuel, K.: Tropical cyclone risk in bangladesh **72**(1), 27–34 https://doi.org/10.54302/mausam.v72i1.122 . Number: 1. Accessed 2023-07-16

[8] World's Deadliest Tropical Cyclone Was 50 Years Ago. https://public.wmo.int/en/media/news/world%E2%80%99s-deadliest-tropical-cyclone-was-50-years-ago Accessed 2023-10-23

[9] Kazi, S., Urrutia, I., Van Ledden, M., Laboyrie, J.H., Verschuur, J., Haque Khan, Z.-u., Jongejan, R., Lendering, K., Mancheño, A.G.: Bangladesh: Enhancing Coastal Resilience in a Changing Climate. World Bank. https://doi.org/10.1596/38004 . http://elibrary.worldbank.org/doi/book/10.1596/38004 Accessed 2023-08-25

[10] Khan, M.J.U., Durand, F., Bertin, X., Testut, L., Krien, Y., Islam, A., Pezerat, M., Hossain, S.: Towards an efficient storm surge and inundation forecasting system over the bengal delta: chasing the supercyclone amphan. Natural Hazards and Earth System Sciences **21**(8), 2523–2541 (2021)

[11] Khan, M.J.U., Durand, F., Emanuel, K., Krien, Y., Testut, L., Islam, A.: Storm surge hazard over bengal delta: a probabilistic–deterministic modelling approach. Natural Hazards and Earth System Sciences **22**(7), 2359–2379 (2022)

[12] Emanuel, K., Ravela, S., Vivant, E., Risi, C.: A statistical deterministic approach to hurricane risk assessment. Bulletin of the American Meteorological Society **87**(3), 299–314 (2006)

[13] Emanuel, K., Sundararajan, R., Williams, J.: Hurricanes and global warming: Results from downscaling ipcc ar4 simulations. Bulletin of the American Meteorological Society **89**(3), 347–368 (2008)

[14] Lin, N., Emanuel, K., Oppenheimer, M., Vanmarcke, E.: Physically based assessment of hurricane surge threat under climate change. Nature Climate Change **2**(6), 462–467 (2012)

[15] Lin, N., Lane, P., Emanuel, K.A., Sullivan, R.M., Donnelly, J.P.: Heightened hurricane surge risk in northwest florida revealed from climatological-hydrodynamic modeling and paleorecord reconstruction. Journal of Geophysical Research: Atmospheres **119**(14), 8606–8623 (2014)

[16] Neumann, J.E., Emanuel, K.A., Ravela, S., Ludwig, L.C., Verly, C.: Risks of coastal storm surge and the effect of sea level rise in the red river delta, vietnam. Sustainability **7**(6), 6553–6572 (2015)

[17] Garner, A.J., Mann, M.E., Emanuel, K.A., Kopp, R.E., Lin, N., Alley, R.B., Horton, B.P., DeConto, R.M., Donnelly, J.P., Pollard, D.: Impact of climate change on new york city's coastal flood hazard: Increasing flood heights from the preindustrial to 2300 ce. Proceedings of the National Academy of Sciences **114**(45), 11861–11866 (2017)

[18] Yin, J., Lin, N., Yang, Y., Pringle, W.J., Tan, J., Westerink, J.J., Yu, D.: Hazard assessment for typhoon-induced coastal flooding and inundation in shanghai, china. Journal of Geophysical Research: Oceans **126**(7), 2021–017319 (2021)

[19] Luettich, R.A., Westerink, J.J., Scheffner, N.W., et al.: Adcirc: an advanced three-dimensional circulation model for shelves, coasts, and estuaries. report 1, theory and methodology of adcirc-2dd1 and adcirc-3dl (1992)

[20] Krien, Y., Mayet, C., Testut, L., Durand, F., Tazkia, A., Islam, A., Gopalakrishna, V., Becker, M., Calmant, S., Shum, C., *et al.*: Improved bathymetric dataset and tidal model for the northern bay of bengal. Marine Geodesy **39**(6), 422–438 (2016)

[21] Alam, E., Dominey-Howes, D.: A new catalogue of tropical cyclones of the northern bay of bengal and the distribution and effects of selected landfalling events in bangladesh. International Journal of Climatology **35**(6), 801–835 (2015)

[22] Dube, S., Rao, A., Sinha, P., Murty, T., Bahulayan, N.: Storm surge in the bay of bengal and arabian sea: the problem and its prediction. Mausam **48**(2), 283–304 (1997)

[23] Dube, S., Chittibabu, P., Sinha, P., Rao, A., Murty, T.: Numerical modelling of storm surge in the head bay of bengal using location specific model. Natural Hazards **31**, 437–453 (2004)

[24] Wu, Z., Hu, C., Lin, L., Chen, W., Huang, L., Lin, Z., Yang, S.: Unraveling the strong covariability of tropical cyclone activity between the bay of bengal and the south china sea. npj Climate and Atmospheric Science **6**(1), 180 (2023)

[25] Philip, S., Sparrow, S., Kew, S.F., Van Der Wiel, K., Wanders, N., Singh, R., Hassan, A., Mohammed, K., Javid, H., Haustein, K., *et al.*: Attributing the 2017 bangladesh floods from meteorological and hydrological perspectives. Hydrology and Earth System Sciences **23**(3), 1409–1429 (2019)

[26] Jakobsen, F., Azam, M.H., Ahmed, M.M.Z., Mahboob-ul-Kabir, M.: Cyclone storm surge levels along the bangladeshi coastline in 1876 and 1960–2000. Coastal Engineering Journal **48**(3), 295–307 (2006)

[27] Leijnse, T.W.B., Giardino, A., Nederhoff, K., Caires, S.: Generating reliable estimates of tropical-cyclone-induced coastal hazards along the bay of bengal for current and future climates using synthetic tracks. Natural Hazards and Earth System Sciences **22**(6), 1863–1891 (2022)

[28] Calafat, F.M., Marcos, M.: Probabilistic reanalysis of storm surge extremes in europe. Proceedings of the National Academy of Sciences **117**(4), 1877–1883 (2020)

[29] Knutson, T., Camargo, S.J., Chan, J.C., Emanuel, K., Ho, C.-H., Kossin, J., Mohapatra, M., Satoh, M., Sugi, M., Walsh, K., *et al.*: Tropical cyclones and climate change assessment: Part ii: Projected response to anthropogenic warming. Bulletin of the American Meteorological Society **101**(3), 303–322 (2020)

[30] Kopp, R.E., Oppenheimer, M., O'Reilly, J.L., Drijfhout, S.S., Edwards, T.L., Fox-Kemper, B., Garner, G.G., Golledge, N.R., Hermans, T.H., Hewitt, H.T., et al.: Communicating future sea-level rise uncertainty and ambiguity to assessment users. Nature Climate Change, 1–13 (2023)

[31] Merz, B., Blöschl, G., Vorogushyn, S., Dottori, F., Aerts, J.C., Bates, P., Bertola, M., Kemter, M., Kreibich, H., Lall, U., *et al.*: Causes, impacts and patterns of disastrous river floods. Nature Reviews Earth & Environment **2**(9), 592–609 (2021)

[32] Bates, P.D., Quinn, N., Sampson, C., Smith, A., Wing, O., Sosa, J., Savage, J.,

Olcese, G., Neal, J., Schumann, G., *et al.*: Combined modeling of us fluvial, pluvial, and coastal flood hazard under current and future climates. Water Resources Research **57**(2), 2020–028673 (2021)

[33] Leijnse, T., Ormondt, M., Nederhoff, K., Dongeren, A.: Modeling compound flooding in coastal systems using a computationally efficient reduced-physics solver: Including fluvial, pluvial, tidal, wind-and wave-driven processes. Coastal Engineering **163**, 103796 (2021)

[34] Holland, G.J.: Tropical Cyclone Motion: Environmental Interaction Plus a Beta Effect. Department of Atmospheric Science, Colorado State University, ??? (1982)

[35] Emanuel, K., DesAutels, C., Holloway, C., Korty, R.: Environmental control of tropical cyclone intensity. Journal of the atmospheric sciences **61**(7), 843–858 (2004)

[36] Bhardwaj, P., Singh, O.: Climatological characteristics of bay of bengal tropical cyclones: 1972–2017. Theoretical and Applied Climatology **139**, 615–629 (2020)

[37] Emanuel, K.: Tropical cyclone seeds, transition probabilities, and genesis. Journal of Climate **35**(11), 3557–3566 (2022)

[38] Westerink, J.J., Luettich Jr, R.A., Blain, C.A., Scheffner, N.W.: Adcirc: an Advanced Three-dimensional Circulation Model for Shelves, Coasts, and Estuaries. Report 2. User's Manual for Adcirc-2ddi. ZSCC: 0000180

[39] Pringle, W.J., Wirasaet, D., Roberts, K.J., Westerink, J.J.: Global storm tide modeling with adcirc v55: unstructured mesh design and performance. Geoscientific Model Development **14**(2), 1125–1145 (2021)

[40] Roberts, K.J., Pringle, W.J., Westerink, J.J.: Oceanmesh2d 1.0: Matlab-based software for two-dimensional unstructured mesh generation in coastal ocean modeling. Geoscientific Model Development **12**(5), 1847–1868 (2019)

[41] Roberts, K.J., Pringle, W.J., Westerink, J.J., Contreras, M.T., Wirasaet, D.: On the automatic and a priori design of unstructured mesh resolution for coastal ocean circulation models. Ocean Modelling **144**, 101509 (2019)

[42] Wessel, P., Smith, W.H.: A global, self-consistent, hierarchical, high-resolution shoreline database. Journal of Geophysical Research: Solid Earth **101**(B4), 8741–8743 (1996)

[43] Weatherall, P., Marks, K.M., Jakobsson, M., Schmitt, T., Tani, S., Arndt, J.E., Rovere, M., Chayes, D., Ferrini, V., Wigley, R.: A new digital bathymetric model of the world's oceans. Earth and space Science **2**(8), 331–345 (2015)

[44] Qiu, J., Liu, B., Yang, F., Wang, X., He, X.: Quantitative stress test of compound

coastal-fluvial floods in china's pearl river delta. Earth's Future **10**(5), 2021–002638 (2022)

[45] Shihora, L., Sulzbach, R., Dobslaw, H., Thomas, M.: Self-attraction and loading feedback on ocean dynamics in both shallow water equations and primitive equations. Ocean Modelling **169**, 101914 (2022)

[46] Pringle, W.J., Wirasaet, D., Westerink, J.J.: Modifications to internal tide conversion parameterizations and implementation into barotropic ocean models (2018)

[47] Egbert, G.D., Erofeeva, S.Y.: Efficient inverse modeling of barotropic ocean tides. Journal of Atmospheric and Oceanic technology **19**(2), 183–204 (2002)

[48] Holland, G.J.: An analytic model of the wind and pressure profiles in hurricanes (1980)

[49] Sindhu, B., Unnikrishnan, A.: Characteristics of tides in the bay of bengal. Marine Geodesy **36**(4), 377–407 (2013)

[50] Rose, L., Bhaskaran, P.K.: Tidal variations associated with sea level changes in the northern bay of bengal. Estuarine, Coastal and Shelf Science **272**, 107881 (2022)

[51] Kopp, R.E., Garner, G.G., Hermans, T.H., Jha, S., Kumar, P., Slangen, A., Turilli, M., Edwards, T.L., Gregory, J.M., Koubbe, G., et al.: The framework for assessing changes to sea-level (facts) v1. 0-rc: A platform for characterizing parametric and structural uncertainty in future global, relative, and extreme sea-level change. EGUsphere, 1–34 (2023)

[52] Marsooli, R., Lin, N., Emanuel, K., Feng, K.: Climate change exacerbates hurricane flood hazards along us atlantic and gulf coasts in spatially varying patterns. Nature communications **10**(1), 3785 (2019)

[53] Coles, S., Bawa, J., Trenner, L., Dorazio, P.: An Introduction to Statistical Modeling of Extreme Values vol. 208. Springer, ??? (2001)

[54] Terrell, G.R., Scott, D.W.: Variable kernel density estimation. The Annals of Statistics, 1236–1265 (1992)

[55] Hersbach, H., Bell, B., Berrisford, P., Hirahara, S., Horányi, A., Muñoz-Sabater, J., Nicolas, J., Peubey, C., Radu, R., Schepers, D., *et al.*: The era5 global reanalysis. Quarterly Journal of the Royal Meteorological Society **146**(730), 1999–2049 (2020)

[56] Gelaro, R., McCarty, W., Suárez, M.J., Todling, R., Molod, A., Takacs, L., Randles, C.A., Darmenov, A., Bosilovich, M.G., Reichle, R., *et al.*: The modern-era

retrospective analysis for research and applications, version 2 (merra-2). Journal of climate **30**(14), 5419–5454 (2017)

[57] Lawrence, D.M., Oleson, K.W., Flanner, M.G., Thornton, P.E., Swenson, S.C., Lawrence, P.J., Zeng, X., Yang, Z.-L., Levis, S., Sakaguchi, K., et al.: Parameterization improvements and functional and structural advances in version 4 of the community land model. Journal of Advances in Modeling Earth Systems **3**(1) (2011)

[58] Donner, L.J., Wyman, B.L., Hemler, R.S., Horowitz, L.W., Ming, Y., Zhao, M., Golaz, J.-C., Ginoux, P., Lin, S.-J., Schwarzkopf, M.D., *et al.*: The dynamical core, physical parameterizations, and basic simulation characteristics of the atmospheric component am3 of the gfdl global coupled model cm3. Journal of Climate **24**(13), 3484–3519 (2011)

[59] Collins, W., Bellouin, N., Doutriaux-Boucher, M., Gedney, N., Halloran, P., Hinton, T., Hughes, J., Jones, C., Joshi, M., Liddicoat, S., *et al.*: Development and evaluation of an earth-system model–hadgem2. Geoscientific Model Development **4**(4), 1051–1075 (2011)

[60] Dufresne, J.-L., Foujols, M.-A., Denvil, S., Caubel, A., Marti, O., Aumont, O., Balkanski, Y., Bekki, S., Bellenger, H., Benshila, R., *et al.*: Climate change projections using the ipsl-cm5 earth system model: from cmip3 to cmip5. Climate dynamics **40**, 2123–2165 (2013)

[61] Watanabe, M., Suzuki, T., O'ishi, R., Komuro, Y., Watanabe, S., Emori, S., Takemura, T., Chikira, M., Ogura, T., Sekiguchi, M., *et al.*: Improved climate simulation by miroc5: mean states, variability, and climate sensitivity. Journal of Climate **23**(23), 6312–6335 (2010)

[62] Giorgetta, M.A., Jungclaus, J., Reick, C.H., Legutke, S., Bader, J., Böttinger, M., Brovkin, V., Crueger, T., Esch, M., Fieg, K., *et al.*: Climate and carbon cycle changes from 1850 to 2100 in mpi-esm simulations for the coupled model intercomparison project phase 5. Journal of Advances in Modeling Earth Systems **5**(3), 572–597 (2013)

[63] Swart, N.C., Cole, J.N., Kharin, V.V., Lazare, M., Scinocca, J.F., Gillett, N.P., Anstey, J., Arora, V., Christian, J.R., Hanna, S., *et al.*: The canadian earth system model version 5 (canesm5. 0.3). Geoscientific Model Development **12**(11), 4823–4873 (2019)

[64] Voldoire, A., Saint-Martin, D., Sénési, S., Decharme, B., Alias, A., Chevallier, M., Colin, J., Guérémy, J.-F., Michou, M., Moine, M.-P., *et al.*: Evaluation of cmip6 deck experiments with cnrm-cm6-1. Journal of Advances in Modeling Earth Systems **11**(7), 2177–2213 (2019)

[65] Hourdin, F., Rio, C., Grandpeix, J.-Y., Madeleine, J.-B., Cheruy, F., Rochetin,

N., Jam, A., Musat, I., Idelkadi, A., Fairhead, L., *et al.*: Lmdz6a: The atmospheric component of the ipsl climate model with improved and better tuned physics. Journal of Advances in Modeling Earth Systems **12**(7), 2019–001892 (2020)

[66] Tatebe, H., Ogura, T., Nitta, T., Komuro, Y., Ogochi, K., Takemura, T., Sudo, K., Sekiguchi, M., Abe, M., Saito, F., *et al.*: Description and basic evaluation of simulated mean state, internal variability, and climate sensitivity in miroc6. Geoscientific Model Development **12**(7), 2727–2765 (2019)

[67] Müller, W.A., Jungclaus, J.H., Mauritsen, T., Baehr, J., Bittner, M., Budich, R., Bunzel, F., Esch, M., Ghosh, R., Haak, H., *et al.*: A higher-resolution version of the max planck institute earth system model (mpi-esm1. 2-hr). Journal of Advances in Modeling Earth Systems **10**(7), 1383–1413 (2018)

[68] Yukimoto, S., Kawai, H., Koshiro, T., Oshima, N., Yoshida, K., Urakawa, S., Tsujino, H., Deushi, M., Tanaka, T., Hosaka, M., *et al.*: The meteorological research institute earth system model version 2.0, mri-esm2. 0: Description and basic evaluation of the physical component. Journal of the Meteorological Society of Japan. Ser. II **97**(5), 931–965 (2019)

Appendix A Extended Data

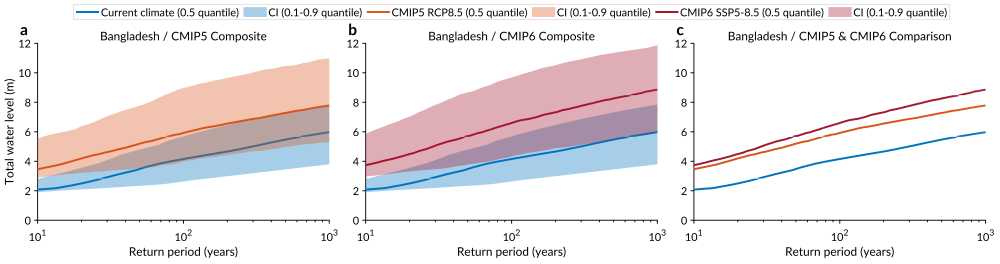

Fig. A1 Bangladesh's coastal flood against return period curves projected by CMIP5 and CMIP6 models at the national scale. **a,** CMIP5 models composite. **b,** CMIP6 models composite. **c,** Comparison between CMIP5 and CMIP6 models. Coastal floods are the total water levels (combined components of the astronomic tide, storm surge, and mean sea level state) relative to the mean sea level of the 1995-2014 baseline. Blue, orange, and red solid lines indicate the ensemble median (0.5 quantiles) for the current climate, CMIP5 RCP8.5 climate, and CMIP6 SSP5-8.5, respectively. Blue, orange, and red shaded areas indicate each estimate's confidence interval (CI, 0.1-0.9 quantile). The current climate period spans from 1981 to 2000, while the future climate period spans from 2081 to 2100.

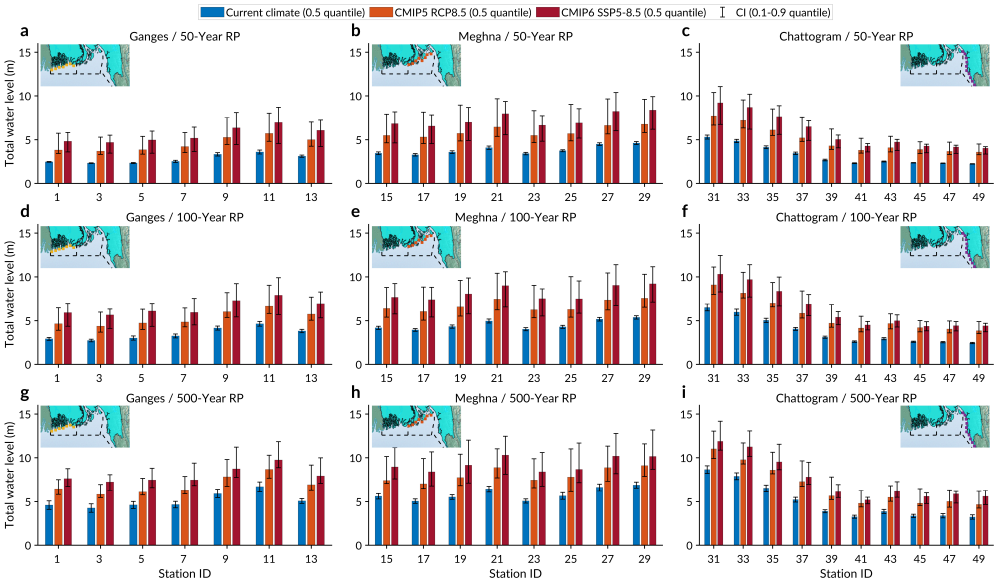

Fig. A2 Bangladesh's 50-year, 100-year, 500-year coastal floods projected by CMIP5 and CMIP6 models at the station scale. Coastal floods are the total water levels (combined components of astronomic tide, storm surge, and mean sea level state) relative to the mean sea level of the 1995-2014 baseline. **a, b, c,** 50-year return period. **d, e, f,** 100-year return period. **g, h, i,** 500-year return period. **a, d, g,** stations located in the Ganges (southwest Bangladesh). **b, e, h,** stations located in the Meghna (middle Bangladesh). **c, f, i,** stations located in the Chattogram (east Bangladesh). Projections are conducted for all 54 stations, but the graph displays only every other station. Blue, orange, and red histograms indicate the ensemble median (0.5 quantiles) for the current climate, CMIP5 RCP8.5 climate, and CMIP6 SSP5-8.5, respectively. Vertical error bars indicate each estimate's confidence interval (CI, 0.1-0.9 quantile). The current climate period spans from 1981 to 2000, while the future climate period spans from 2081 to 2100. Base map sourced from the BDP 2100 (Baseline Volume 1, pg. 403), Humanitarian Data Exchange, World Bank, ESRI ArcGIS, Maxar, Earthstar Geographics, USDA FSA, USGS, Aerogrid, IGN, IGP, and the GIS User Community.

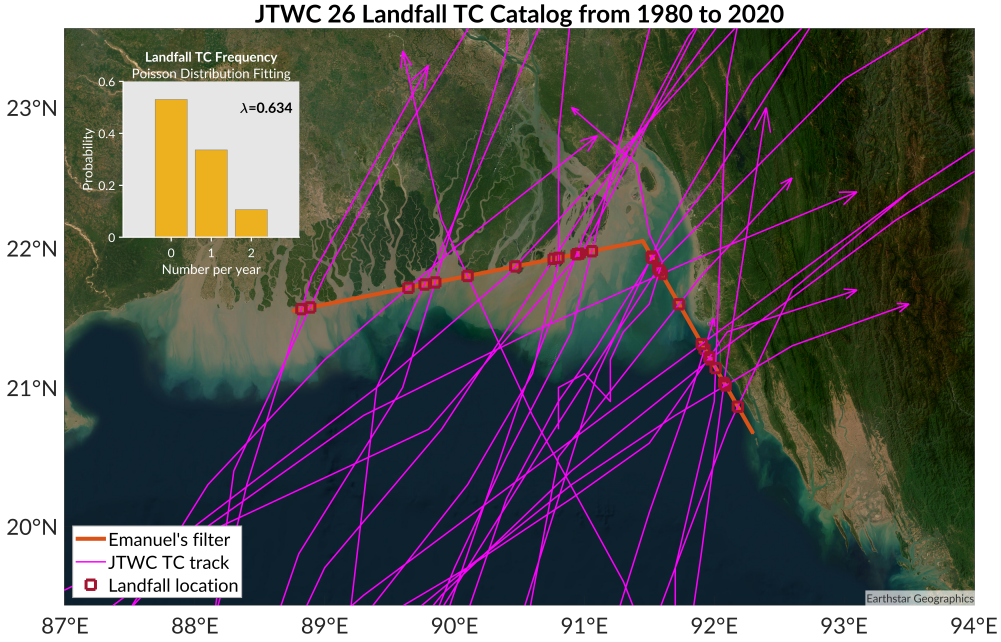

Fig. A3 Annual TC frequency analyzed using 26 JTWC TCs that made landfall in Bangladesh from 1980 to 2020. These magenta lines with arrows indicate the TC's track. The bold orange two-segment lines indicate Emanuel's filter used in generating synthetic TC tracks affecting Bangladesh. Red squares on the filter indicate TC landfall locations. The upper left panel displays the annual TC frequency estimation ($\lambda = 0.634$) by fitting a Poisson distribution with the annual occurrence rate. Base map sourced from the ESRI ArcGIS, Maxar, Earthstar Geographics, USDA FSA, USGS, Aerogrid, IGN, IGP, and the GIS User Community.

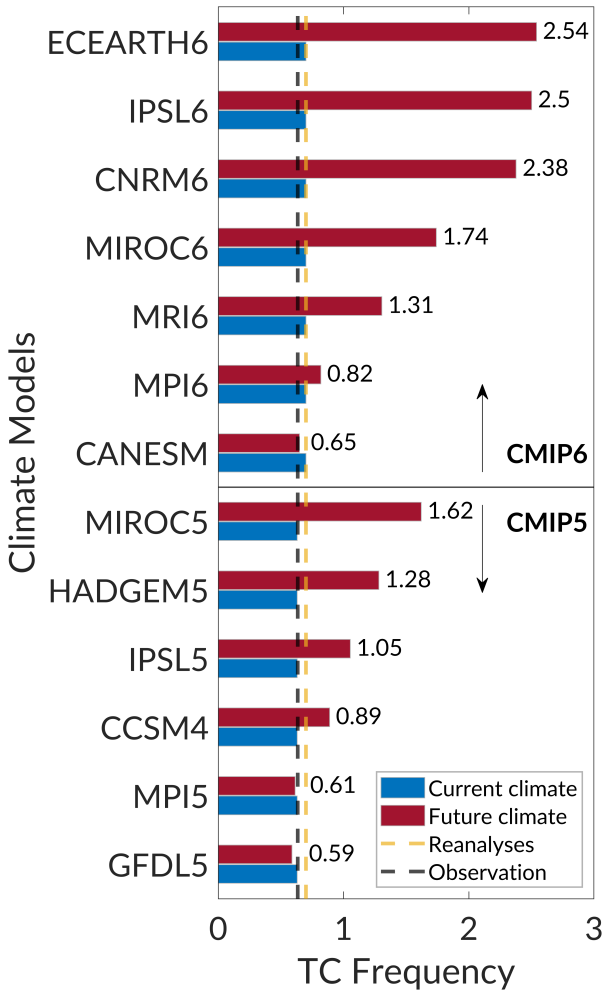

Fig. A4 Projected annual TC frequency (without bias correction) from CMIP5 (lower panel) and CMIP6 (upper panel) models. The blue and red horizontal bar lengths indicate projected annual TC frequency in current and future climates (RCP8.5 for CMIP5, SSP5-8.5 for CMIP6), respectively. The vertical yellow and black dash lines indicate the annual TC frequency estimated based on climate reanalyses (including ECMWF/ERA5 and GMAO/MERRA2) and JTWC historical observation. The bias-corrected annual TC frequency is summarized in our Method (Synthetic TC generation).

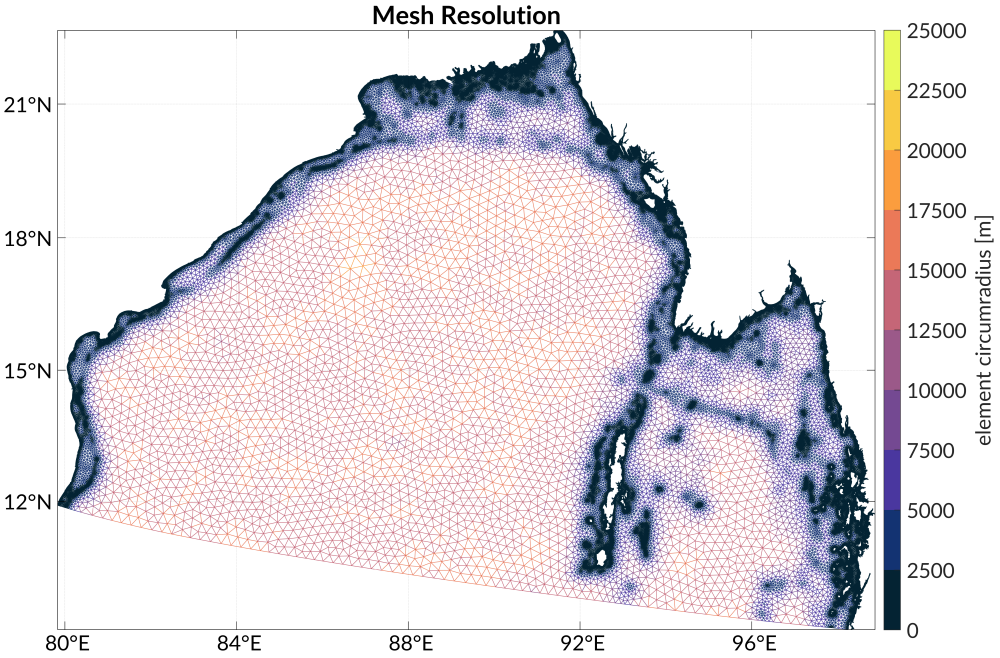

Fig. A5 Mesh triangulation and resolution (showed on a "miller" projection) for the northern Bay of Bengal domain.

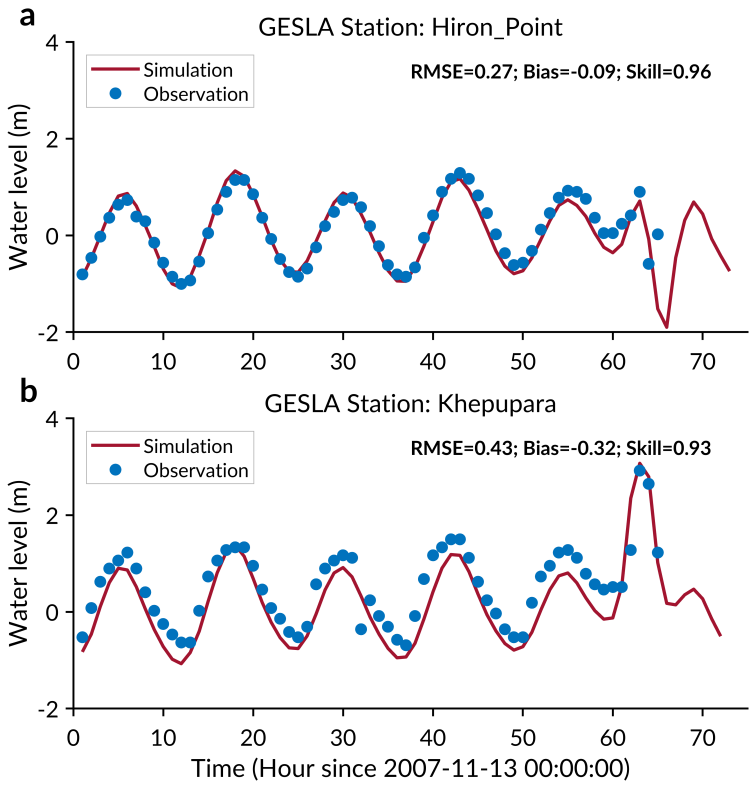

Fig. A6 Comparison between modeled (red lines) and observed (blue points) total water levels at station Hiron_point (a) and Khepupara (b) for the validation of Sidr-induced coastal flood.

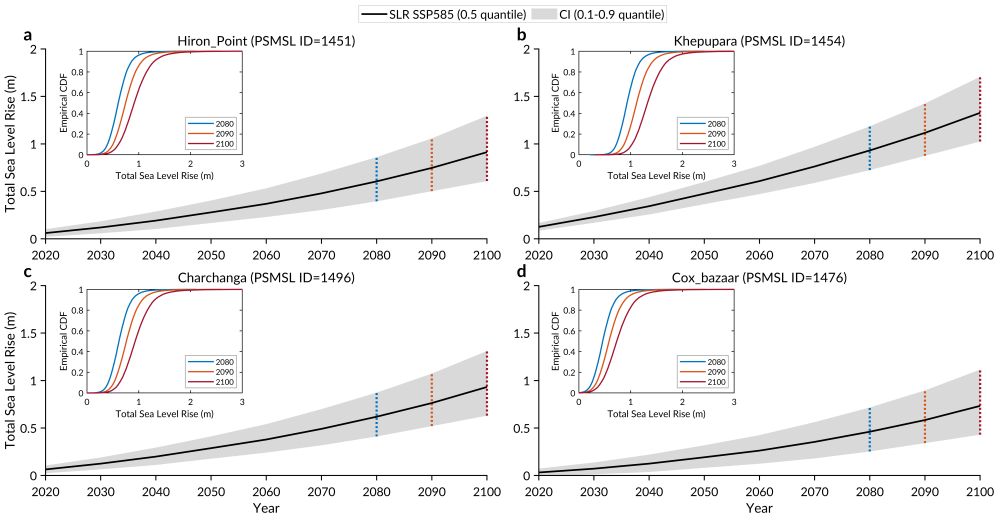

Fig. A7 IPCC AR6 relative sea-level projections from 2020 to 2100 for station Hiron_point (a), Khepupara (b), Charchanga (c) and Cox_bazaar (d). The black solid lines indicate the median value (0.5 quantile) of the projected values of total sea level rise, while the gray shaded areas indicate the confidence interval (quantile 0.1-0.9). The upper left panel of each subplot displays the CDF curve of the 20000 Monte Carlo samples for years 2080, 2090, and 2100, respectively.

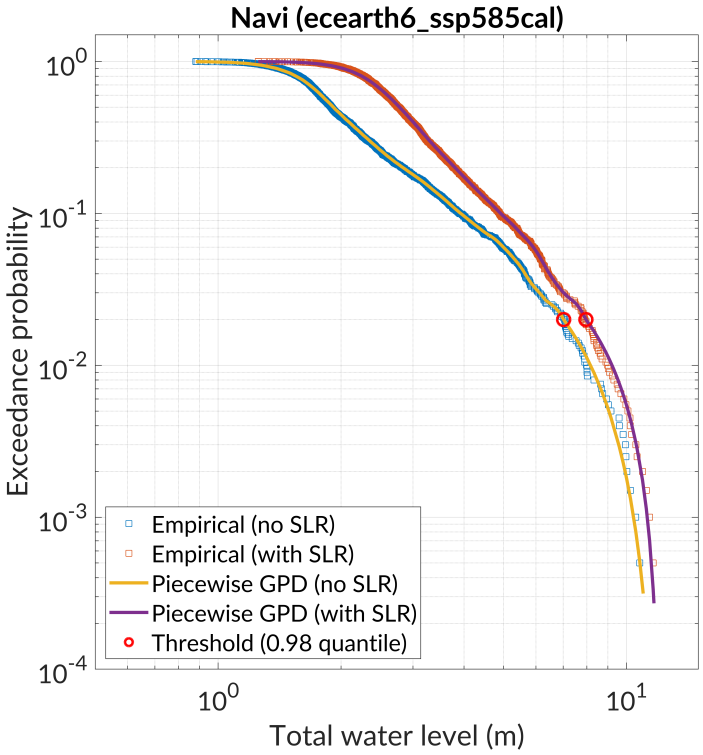

Fig. A8 An example of exceedance probability fitting curve with (purple line) and without (yellow line) considering the effect of SLR at station Navi with ID=31 under ECEARTH6 SSP5-8.5 scenario. The square dots represent the empirical exceedance probability for each total water level, while the solid line indicates the fitted exceedance probability curve using the piecewise Kernel-GPD estimation method. The red circle highlighted in bold indicates the threshold (quantile) used to segment the dataset for fitting the GPD model in the tail, while a kernel estimation is used in the remaining part. We performed the same fitting at all stations under all scenarios.

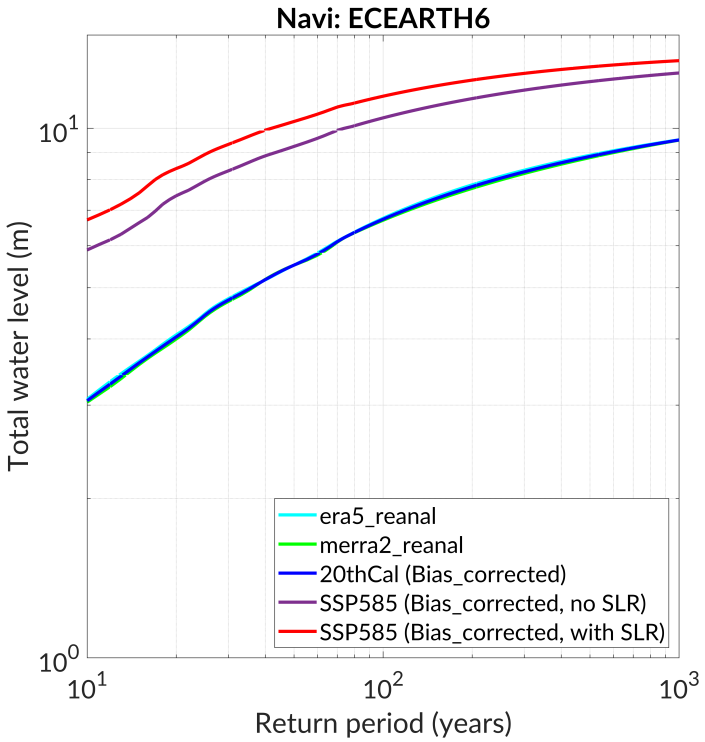

Fig. A9 An example of the bias correction for the total water level against return period curves with (red line) and without (purple line) considering the effect of SLR at station Navi. The cyan, green, and blue lines represent the total water level and return period curves under the ERA5, MERRA2, and ECEARTH6 20th, respectively; these three lines overlap because we calibrated the ECEARTH6 20th to the averaged ERA5 and MERRA2 reanalyses. We performed the same bias correction procedure for all CMIP models at all stations.

Table A1 List of Climate reanalysis product, CMIP5, and CMIP6 model used in downscaling of tropical cyclones, including average horizontal resolution and principal reference.

Institution	ID	Model name	Model type	Atmospheric resolution	Reference
European Center for Medium-Range Weather Forecasts	ECMWF	ERA5	Reanalyses	0.25° × 0.25°	[55]
NASA's Global Modeling and Assimilation Office	GMAO	MERRA2	Reanalyses	0.5° × 0.625°	[56]
National Center for Atmospheric Research	NCAR	CCSM4	CMIP5	1.25° × 0.94°	[57]
NOAA Geophysical Fluid Dynamics Laboratory	GFDL	CM3	CMIP5	2.5° × 2.0°	[58]
Met Office Hadley Center	MOHC	HADGEM2-ES	CMIP5	1.875° × 1.25°	[59]
Institute Pierre Simon Laplace	IPSL	CM5A-LR	CMIP5	3.75° × 1.89°	[60]
Atmosphere and Ocean Research Institute (The University of Tokyo), National Institute for Environmental Studies, and Japan Agency for Marine-Earth Science and Technology	MIROC	MIROC5	CMIP5	1.41° × 1.40°	[61]
Max Planck Institute	MPI	MPI-ESM-MR	CMIP5	1.875° × 1.865°	[62]
Canadian Center for Climate Modeling and Analysis	CANESM	CanESM5	CMIP6	2.8° × 2.8°	[63]
Center National de Recherches Météorologiques	CNRM	CNRM-CM6-1	CMIP6	1.4° × 1.4°	[64]
EC-Earth consortium	ECEARTH	EC-Earth3	CMIP6	0.7° × 0.7°	
Institute Pierre Simon Laplace	IPSL	IPSL-CM6A-LR	CMIP6	1.25° × 2.5°	[65]
Center for Climate System Research; University of Tokyo; Japan Agency for Marine-Earth Science and Technology; National Institute for Environmental Studies	MIROC	MIROC6	CMIP6	1.4° × 1.4°	[66]
Max Planck Institute	MPI	MPI-ESM1-2-HR	CMIP6	0.94° × 0.94°	[67]
Meteorological Research Institute (Japan)	MRI	MRI-ESM2-0	CMIP6	1.12° × 1.125°	[68]

Appendix B Supplementary

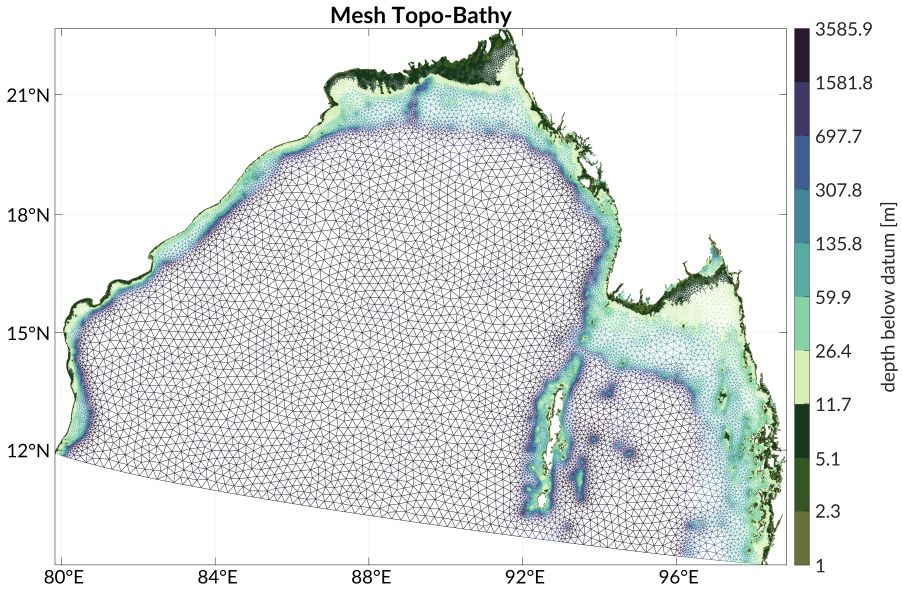

Fig. B10 Mesh triangulation and depth (use a colormap to plot the color in log space) for the BoB model.

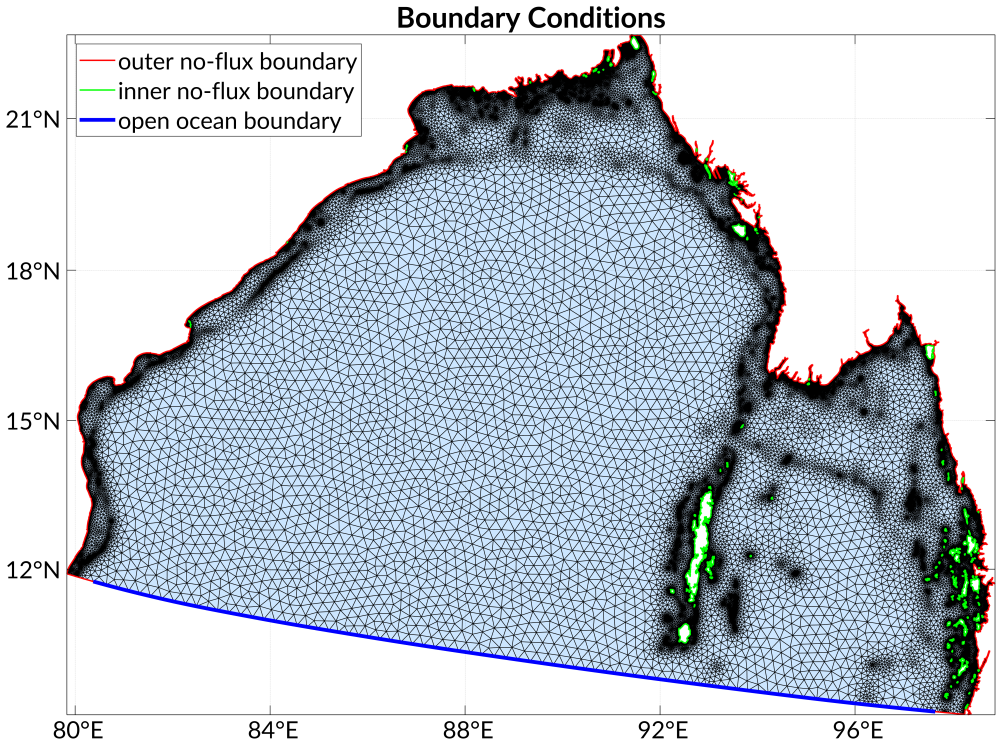

Fig. B11 Mesh triangulation and open boundaries for the BoB model.

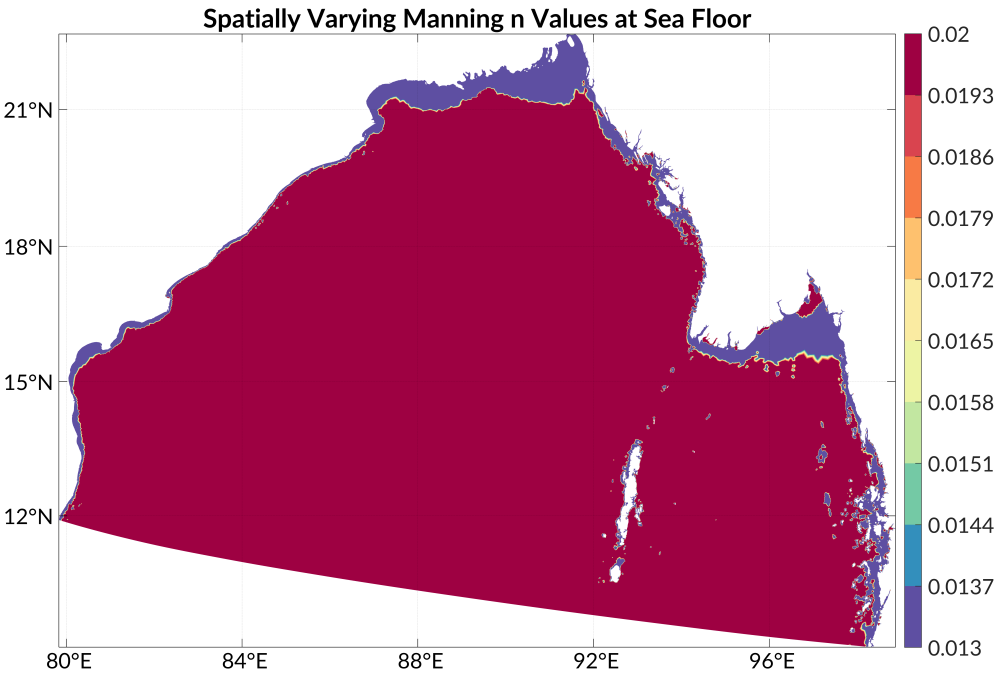

Fig. B12 Spatially varying Manning's-N values at sea floor for the BoB model.

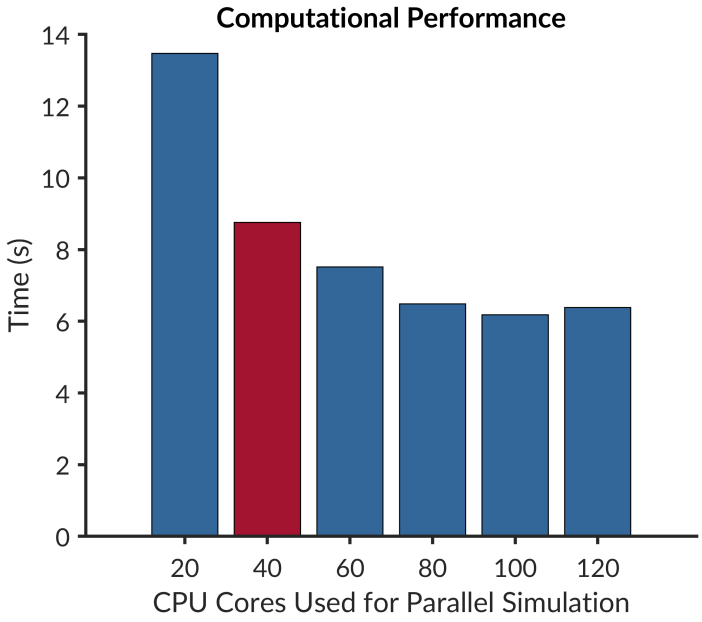

Fig. B13 Computational performance evaluation of the BoB model tested by a synthetic TC track for increasing CPUs. All the synthetic TCs are finally simulated using 40 CPU (marked red) cores for parallel.

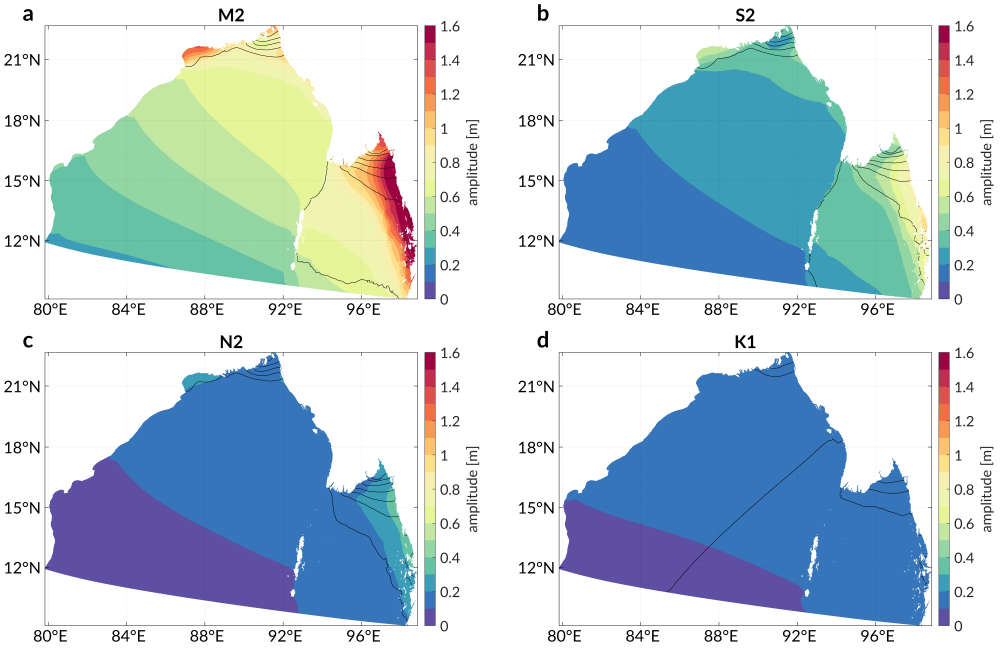

Fig. B14 Amplitude (background color, unit: m) and phase (cotidal lines with 30 increments) responses of the M_2 (a), S_2 (b), N_2 (c), K_1 (d) tidal waves. Five tidal constitutes are activated in the harmonic analysis for the astronomic tide validation; only the first four tidal constitutes' results are shown here.

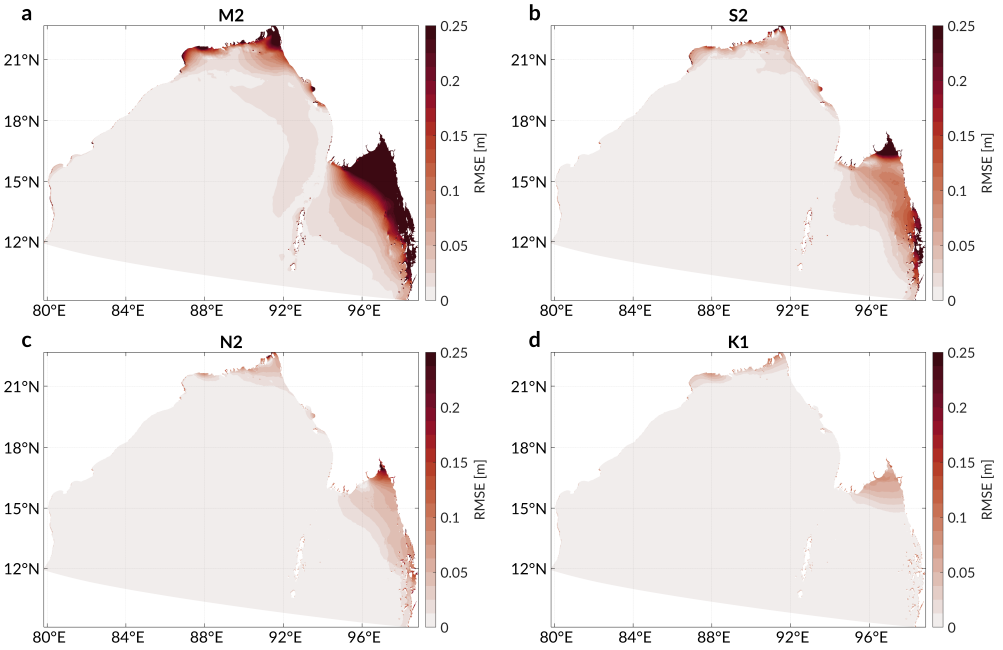

Fig. B15 Root-mean-square error (m) of our model setup against the TPXO9-Altas for the M_2 (a), S_2 (b), N_2 (c) and K_1 (d) tidal waves. Five tidal constituents are activated in the harmonic analysis for the astronomic tide validation; only the first four tidal constituents' results are shown here.

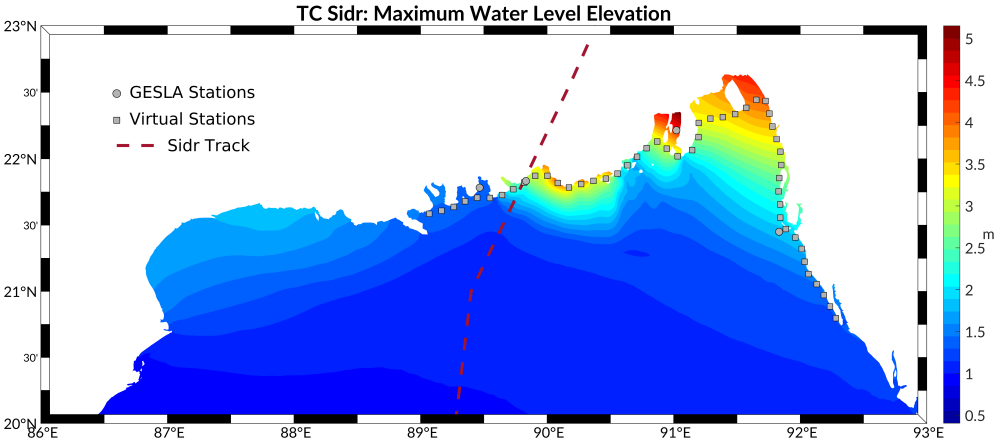

Fig. B16 Maximum water level elevation during Sidr make landfall to Bangladesh.

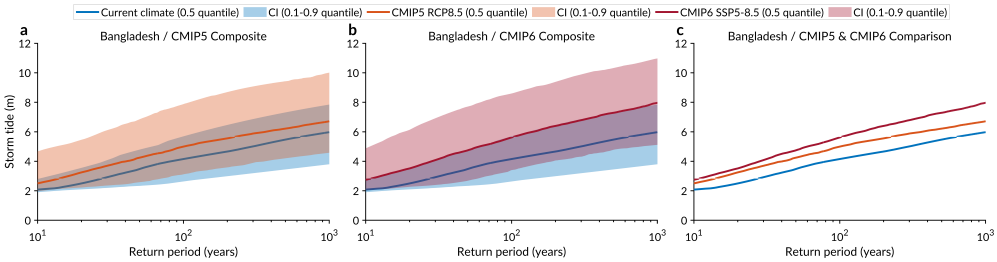

Fig. B17 Bangladesh's storm tide against return period curves projected by CMIP5 and CMIP6 models at the national scale. Storm tides are the water level elevations (only combining components of astronomic tide and storm surge) relative to the mean sea level of the 1995-2014 baseline. **a,** CMIP5 models composite. **b,** CMIP6 models composite. **c,** Comparison between CMIP5 and CMIP6 models. Blue, orange, and red solid lines indicate the ensemble median (0.5 quantile) for the current climate, CMIP5 RCP8.5 climate, and CMIP6 SSP5-8.5, respectively. Blue, orange, and red shaded areas indicate each estimate's confidence interval (CI, 0.1-0.9 quantile). The current climate period spans from 1981 to 2000, while the future climate period spans from 2081 to 2100.

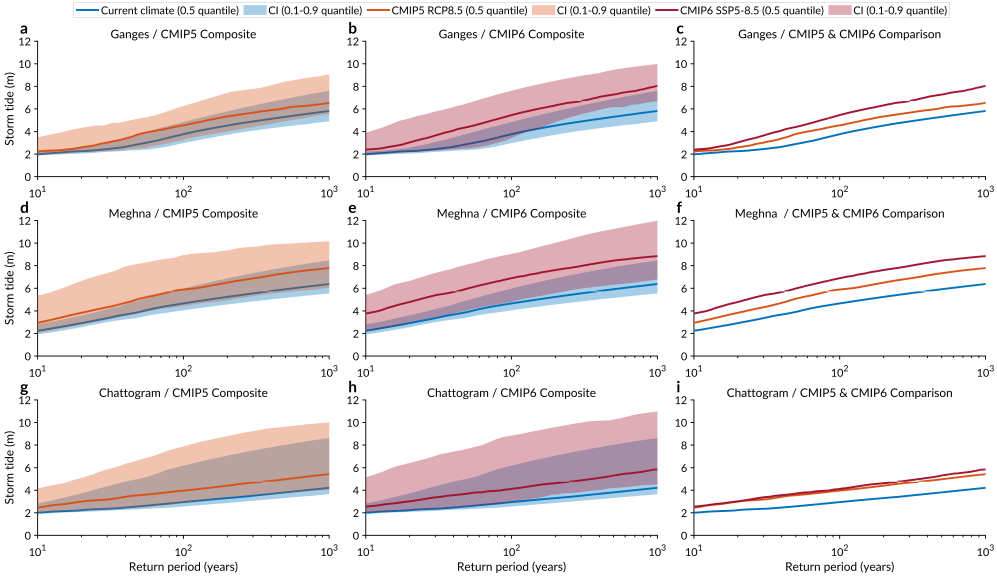

Fig. B18 Bangladesh's storm tide against return period curves projected by CMIP5 and CMIP6 models at the regional scale. Storm tides are the water level elevations (only combining components of astronomic tide and storm surge) relative to the mean sea level of the 1995-2014 baseline. **a, b, c,** Projections for the Ganges (southwest Bangladesh). **d, e, f,** Projections for the Meghna (middle Bangladesh). **g, h, i,** Projections for the Chattogram (east Bangladesh). **a, d, g,** CMIP5 models composite. **b, e, h,** CMIP6 models composite. **c, f, i,** Comparison between CMIP5 and CMIP6 models. Blue, orange, and red solid lines indicate the ensemble median (0.5 quantile) for the current climate, CMIP5 RCP8.5 climate, and CMIP6 SSP5-8.5, respectively. Blue, orange, and red shaded areas indicate the confidence interval (i.e., 0.1-0.9 quantile) for each of these estimates. The current climate period spans from 1981 to 2000, while the future climate period spans from 2081 to 2100.

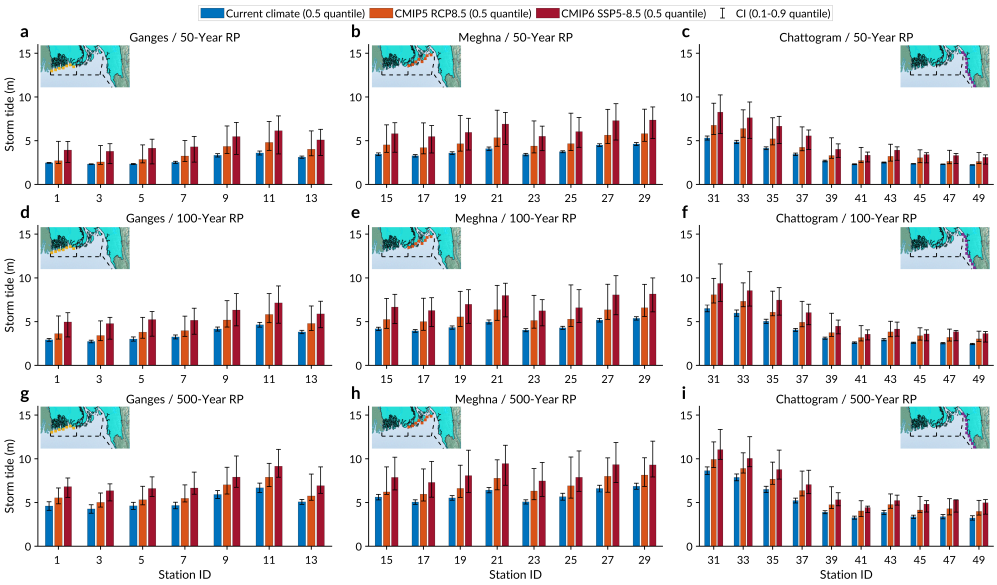

Fig. B19 Bangladesh's 50-year, 100-year, 500-year storm tides projected by CMIP5 and CMIP6 models at the station scale. Storm tides are the water level elevations (only combining components of astronomic tide and storm surge) relative to the mean sea level of the 1995-2014 baseline. **a, b, c,** 50-year return period. **d, e, f,** 100-year return period. **g, h, i,** 500-year return period. **a, d, g,** stations located in the Ganges (southwest Bangladesh). **b, e, h,** stations located in the Meghna (middle Bangladesh). **c, f, i,** stations located in the Chattogram (east Bangladesh). Projections are conducted for all 54 stations, but the graph displays only every other station. Blue, orange, and red histograms indicate the ensemble median (0.5 quantile) for the current climate, CMIP5 RCP8.5, and CMIP6 SSP5-8.5 climate, respectively. Vertical error bars indicate each estimate's confidence interval (CI, 0.1-0.9 quantile). The current climate period spans from 1981 to 2000, while the future climate period spans from 2081 to 2100. Base map sourced from the BDP 2100 (Baseline Volume 1, pg. 403), Humanitarian Data Exchange, World Bank, ESRI ArcGIS, Maxar, Earthstar Geographics, USDA FSA, USGS, Aerogrid, IGN, IGP, and the GIS User Community.

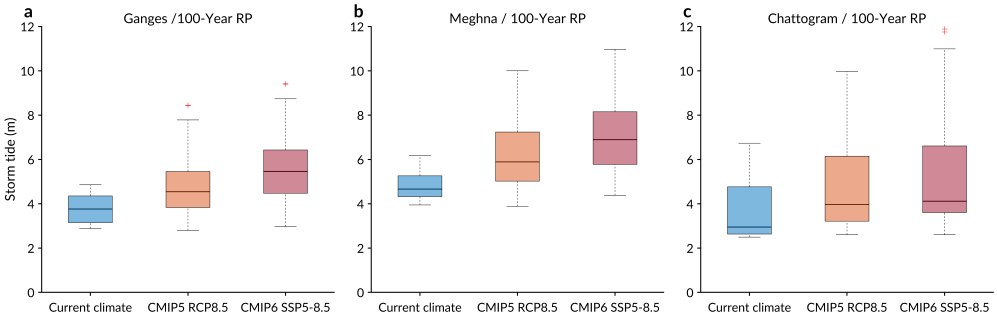

Fig. B20 Statistics for 100-year storm tides (without SLR) for the Ganges, Meghna, and Chattogram regions.

Table B2 Detailed information about the virtual and GESLA stations along the Bangladesh coast.

ID	Lon	Lat	Name	Location	ID	Lon	Lat	Name	Location
1	89.0690124	21.5854591	Alex	Ganges	28	91.3884806	22.312742	Lubna	Meghna
2	89.166293	21.6086212	Ali	Ganges	29	91.4855022	22.3358424	Malai	Meghna
3	89.2618475	21.6374707	Amro	Ganges	30	91.5727113	22.3830833	Mitteldorf	Meghna
4	89.3519373	21.6802386	Bakli	Ganges	31	91.652238	22.4436514	Navi	Chattogram
5	89.4475076	21.7066318	Barbehenn	Ganges	32	91.7268907	22.4347949	Nick	Chattogram
6	89.5471717	21.7052361	Basha	Ganges	33	91.7564113	22.3395824	Nishant	Chattogram
7	89.644022	21.7271781	Castillo	Ganges	34	91.7800037	22.2425041	Paco	Chattogram
8	89.7331994	21.7709685	Chen	Ganges	35	91.8143059	22.148696	Pitts	Chattogram
9	89.8195397	21.8214198	Chew	Ganges	36	91.8429101	22.0530798	Rodi	Chattogram
10	89.9057356	21.8721172	Dada	Ganges	37	91.8496498	21.9537402	Jiangchao	Chattogram
11	90.0015167	21.8720089	Didi	Ganges	38	91.83439	21.8551361	Saha	Chattogram
12	90.0848174	21.8182692	Duyck	Ganges	39	91.829805	21.7554847	Sai	Chattogram
13	90.1731304	21.7838998	Edison	Ganges	40	91.8405295	21.6561052	Salas	Chattogram
14	90.2687542	21.8099768	Emanuel	Ganges	41	91.8418013	21.5564125	Seybold	Chattogram
15	90.3658168	21.8339145	Finn	Meghna	42	91.8856959	21.4709733	Sonia	Chattogram
16	90.4644153	21.8504308	Fiyi	Meghna	43	91.9618326	21.4064959	Tagade	Chattogram
17	90.5564202	21.8883925	Gabe	Meghna	44	92.0119427	21.3210051	Thelonius	Chattogram
18	90.6336208	21.9512461	Goran	Meghna	45	92.0348013	21.2240663	Trautner	Chattogram
19	90.7103935	22.0153038	Grace	Meghna	46	92.0657374	21.1308986	Tswift	Chattogram
20	90.7861956	22.0803504	Hayek	Meghna	47	92.1303292	21.055069	Yamaguchi	Chattogram
21	90.8696544	22.1299695	Ilish	Meghna	48	92.1863032	20.9722584	Yang	Chattogram
22	90.9461398	22.0760626	Iris	Meghna	49	92.2351253	20.8850721	Zhuchang	Chattogram
23	91.0310217	22.0190889	Runge	Meghna	50	92.2822905	20.7968937	Ziwei	Chattogram
24	91.1459135	22.0650456	Kutta	Meghna	51	89.467	21.783	Hiron_Point	Ganges
25	91.1964659	22.1630866	Kyra	Meghna	52	89.833	21.833	Khepupara	Ganges
26	91.1983726	22.2695462	Langlois	Meghna	53	91.0218303	22.2151709	Charchanga	Meghna
27	91.2890317	22.3023262	Lee	Meghna	54	91.833	21.45	Coxs_Bazaar	Chattogram

Table B3 Parameters used to distribute element resolution spatially

Edge_length function	Parameter
min_reso	1 km
max_reso	20 km
wave length	30
slope	10
filter	-50
grade	0.35
feature width	3